Journal Pre-proof

Ceramide ratios are affected by cigarette smoke but not heat-not-burn or e-vapor aerosols across four independent mouse studies

Oksana Lavrynenko, Bjoern Titz, Sophie Dijon, Daniel Dos Santos, Catherine Nury, Thomas Schneider, Emmanuel Guedj, Justyna Szostak, Athanasios Kondylis, Blaine Phillips, Kim Ekroos, Florian Martin, Manuel C. Peitsch, Julia Hoeng, Nikolai V. Ivanov

PII: S0024-3205(20)31506-X

DOI: https://doi.org/10.1016/j.lfs.2020.118753

Reference: LFS 118753

To appear in: *Life Sciences*

Received date: 20 August 2020

Revised date: 3 November 2020

Accepted date: 10 November 2020

Please cite this article as: O. Lavrynenko, B. Titz, S. Dijon, et al., Ceramide ratios are affected by cigarette smoke but not heat-not-burn or e-vapor aerosols across four independent mouse studies, *Life Sciences* (2018), https://doi.org/10.1016/j.lfs.2020.118753

This is a PDF file of an article that has undergone enhancements after acceptance, such as the addition of a cover page and metadata, and formatting for readability, but it is not yet the definitive version of record. This version will undergo additional copyediting, typesetting and review before it is published in its final form, but we are providing this version to give early visibility of the article. Please note that, during the production process, errors may be discovered which could affect the content, and all legal disclaimers that apply to the journal pertain.

© 2018 Published by Elsevier.

Journal Pre-proof

Ceramide ratios are affected by cigarette smoke but not heat-not-burn or e-vapor aerosols across four independent mouse studies

Oksana Lavrynenko[1,*‡], Bjoern Titz[1‡], Sophie Dijon[1], Daniel Dos Santos [1], Catherine Nury[1], Thomas Schneider[1], Emmanuel Guedj[1], Justyna Szostak[1], Athanasios Kondylis[1], Blaine Phillips[2], Kim Ekroos[3], Florian Martin[1], Manuel C. Peitsch[1], Julia Hoeng[1] and Nikolai V. Ivanov[1]

[1] PMI R&D, Philip Morris Products S.A., Quai Jeanrenaud 5, CH-2000 Neuchâtel, Switzerland
[2] Philip Morris International Research Laboratories Pte. Ltd., Science Park II, 117406, Singapore
[3] Lipidomics Consulting Ltd., Irisviksvägen 31D, 02230 Esbo, Finland
[‡] Equal contribution
[*] Correspondence: Oksana.Lavrynenko@pmi.com

Received: date; Accepted: date; Published: date

Abstract

Aims

Smoking is an important risk factor for the development of chronic obstructive pulmonary disease and cardiovascular diseases. This study aimed to further elucidate the role of ceramides, as a key lipid class dysregulated in disease states.

Main methods

In this article we developed and validated LC–MS/MS method for ceramides (Cer(d18:1/16:0), Cer(d18:1/18:0), Cer(d18:1/24:0) and Cer(d18:1/24:1(15Z)) for the absolute quantification. We deployed it together with proteomics and transcriptomic analysis to assess the effects of cigarette smoke (CS) from the reference cigarette as well as aerosols from heat-not-burn (HnB) tobacco and e-vapor products in apolipoprotein E-deficient (ApoE$^{-/-}$) mice over several time points.

Key findings

In the lungs, CS exposure substantially elevated the ratios of Cer(d18:1/24:0) and Cer(d18:1/24:1) to Cer(d18:1/18:0) in two independent ApoE$^{-/-}$ mouse inhalation studies. Data from previous studies, in both ApoE$^{-/-}$ and wild-type mice, further confirmed the reproducibility of this finding. Elevation of these ceramide ratios was also observed in plasma/serum, the liver, and—for the Cer(d18:1/24:1(15Z)) to Cer(d18:1/18:0) ratio—the abdominal aorta. Also, the levels of acid ceramidase (Asah1) and glucocerebrosidase (Gba)—lysosomal enzymes involved in the hydrolysis of glucosylceramides—were consistently elevated in the lungs after CS exposure. In contrast, exposure to HnB tobacco product and e-vapor aerosols did not induce significant changes in the ceramide profiles or associated enzymes.

Significance

Our work in mice contributes to the accumulating evidence on the importance of ceramide ratios as biologically relevant markers for respiratory disorders, adding to their already demonstrated role in cardiovascular disease risk assessment in humans

Keywords: Ceramides; Lipidomics; COPD; Cigarette smoke; Heat-not-burn tobacco product; E-cigarettes

Introduction

Smoking causes several diseases, including chronic obstructive pulmonary disease (COPD) and cardiovascular diseases [1, 2]. Smoking cessation is the most effective way to reduce the risk of developing the smoking-related diseases [3]; however, switching to less harmful modified risk tobacco product (MRTP) can be an alternative for adult smokers who otherwise would continue to smoke. Potential MRTPs include electronic cigarettes (ECIG) and heat-not-burn (HnB) tobacco products. Tobacco Heating System (THS) 2.2 and Carbon Heating Tobacco System (CHTP) 1.2 are two HnB tobacco products developed by Phillip Morris International [4, 5], which were designed as electronic devices that heat tobacco in a controlled manner. ECIGs are devices that aerosolize liquids composed of the mixture of nicotine and flavors in carrier substances. Both HnB products and ECIGs release harmful chemicals and carcinogenic metabolites at substantially lower levels than cigarettes [6-11].

In the lungs, cigarette smoke (CS) induces an oxidative stress responses, inflammation, and structural tissue changes [12, 13]. In both animal and clinical studies, CS exposure has been associated with a far-reaching impact on the lung lipidome. This includes its effects on surfactant lipids, lipid signaling mediators, and structural lipids as well as ceramides. In the lungs, ceramide accumulation induces epithelial cell damage sustaining inflammation [14]. Moreover, ceramides are engaged in signaling cascades required for physiological immune responses and resolution of inflammation [15]. Therefore, ceramides are currently attracting major interest as potential disease biomarkers [16, 17] for diverse pathological conditions such as cardiovascular diseases [18, 19], cancer [20], neurodegeneration [21], diabetes [22], microbial pathogenesis [23], obesity, and inflammation [24].

In the context of CS exposure, ceramides have been implicated in endothelial barrier disruption [25], lung emphysema [26], inflammation [27, 28] and altered myocardial mitochondrial function [29]. Lipidomics profiling of induced sputum samples highlighted increased levels of 28 ceramides in smokers with COPD versus smokers without COPD [30]. The differences between smokers without COPD and never-smokers only showed the significant changes in glycosphingolipids. In a recent comprehensive lipid profiling experiment in C57BL/6 and ApoE$^{-/-}$ mice, we found that CS exposure caused upregulation of very-long-chain ceramides and downregulation of long-chain ceramides while the exposure to aerosols of THS 2.2 and a prototype MRTP was associated with much more limited effects on these ceramides[13].

Here, we evaluated the impact of four ceramides as markers of the biological response to CS exposure in mice. We developed and validated a high-throughput method for quantification of Cer(d18:1/16:0), Cer(d18:1/18:0), Cer(d18:1/24:0), and Cer(d18:1/24:1(15Z)). We accessed the ceramide response to CS in two separate inhalation toxicology studies with ApoE$^{-/-}$ mice as a well-suited model for simultaneous assessment of respiratory and cardiovascular (atherosclerotic plaque formation) effects [31, 32]. These case studies allowed us to evaluate the reproducibility of previous findings as well as to determine how ceramide levels were affected in different tissues and plasma. Finally, these studies allowed us to compare the effects of CS exposure with those of exposure to aerosols from heat not burned products (ApoE$^{-/-}$ HnB study) [33], and exposure to e-vapor product aerosol (ApoE$^{-/-}$ e-vapor study) [34].

2. Materials and Methods

Standards and chemicals

Bovine serum albumin, SigMatrix serum diluent, ammonium bicarbonate bio ultra-grade, 2-propanol LC-MS grade, water LC-MS grade, acetonitrile LC-MS grade, NIST 1950 human plasma were obtained from Sigma-Aldrich (Buchs SG, Switzerland). Butanol ACS grade, methanol LC-MS grade, dichloromethane HPLC grade, ethyl acetate LC-MS grade, acetic acid HPLC grade, and chloroform HPLC grade were provided by Honeywell (Seelze, Germany). Ammonium acetate LC-MS grade was purchased from Thermo Fisher (Rockford, IL, USA). Quick Start Bradford 1X Die Reagent was purchased from BioRad (Cressier, Switzerland). Ceramide LIPIDOMIX® Mass Spec Standard and Deuterated Ceramide LIPIDOMIX® Mass Spec Standard were purchased from Avanti (Alabama, USA). Formic acid LC-MS grade was purchased from Merck (Darmstadt, Germany) and pooled female plasma from Seralab (Sussex, UK).

ApoE$^{-/-}$ mouse studies

Details on the two exposure studies in ApoE$^{-/-}$ mice are reported in Phillips *et al.* [33] (ApoE$^{-/-}$ HnB study) and Szostak *et al.* [34] (ApoE$^{-/-}$ e-vapor study). Figure 1A illustrates the exposure design and analyzed biological matrices for the ceramide assay. Table 4 summarizes the exposure regimens for the two studies. The table also contains information on two previous exposure studies (in ApoE$^{-/-}$ and wild-type (WT) C57Bl6 mice), which we used to further assess the reproducibility of the findings [13, 35, 36].

All procedures involving animals were performed in a facility accredited by the Association for Assessment and Accreditation of Laboratory Animal Care International and licensed by the Agri-Food & Veterinary Authority of Singapore, with approval from an Institutional Animal Care and Use Committee and in compliance with the National Advisory Committee for Laboratory Animal Research Guidelines on the Care and Use of Animals for Scientific Purposes (NACLAR, 2004).

Briefly, female B6.129P2-Apoe^{tm1Unc} N11 ApoE$^{-/-}$ mice, bred under specific-pathogen-free conditions, were obtained from Taconic Biosciences (Rensselaer, NY, USA). 3R4F reference cigarettes were purchased from the University of Kentucky. CHTP 1.2 uses a pressed carbon heat source to heat a tobacco plug in a specially designed stick to produce a nicotine-containing aerosol. THS 2.2 comprises a single-use disposable stick containing a tobacco plug inserted into a holder, which contains a battery, electronics for temperature control, a heating element, and a stick extractor [4, 10, 37, 38]. The holder heats the tobacco electrically in a controlled way to ensure that combustion temperatures are not reached. More details on CHTP 1.2 and THS 2.2 have been published previously [10, 11]. The e-vapor product liquid formulations assessed in this study were PG/VG (CARRIER), PG/VG/nicotine (BASE), and PG/VG/nicotine/flavoring mix (TEST) (Supplementary Table S21).

Mainstream CS smoke, 3R4F cigarettes, aerosols from CHTP 1.2 and THS 2.2, and e-vapor product aerosols were generated as described by Phillips et al. [33] and Szostak *et al.* [34] (see Table 4).

In the ApoE$^{-/-}$ HnB and ApoE$^{-/-}$ e-vapor studies, dissections were performed after 3 and 6 months of exposure. Tissues were collected 16–24 h after exposure, snap-frozen in liquid nitrogen, and stored at -80°C before initiation the lipidomics workflow. The present study analyzed samples from 9 and 10 animals from the "omics" dissection groups of the ApoE$^{-/-}$ HnB and e-vapor studies, respectively.

Journal Pre-proof

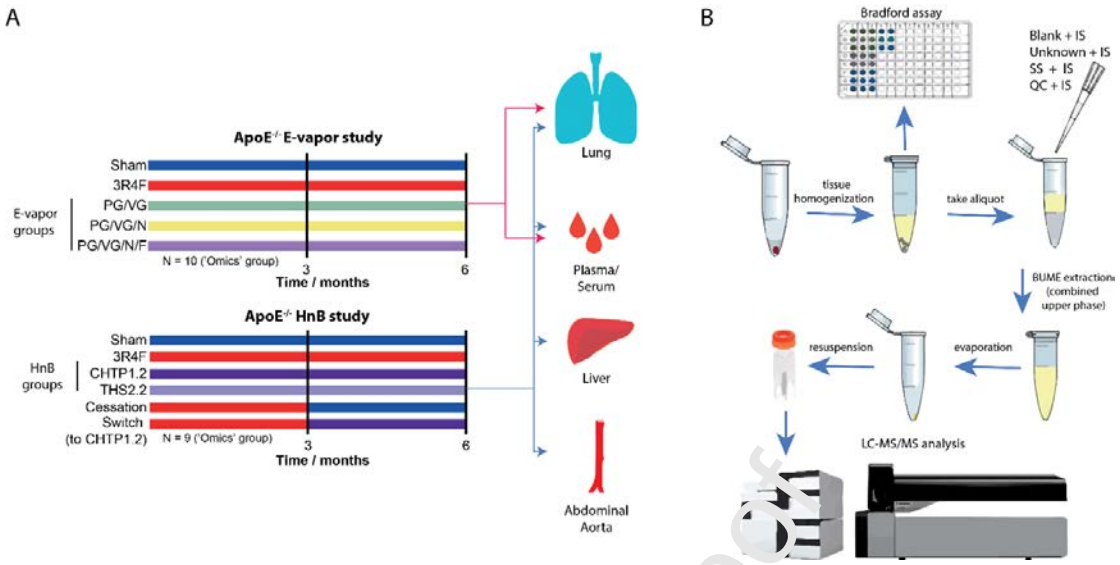

Figure 1. Study design of the ApoE$^{-/-}$ studies and schematic representation of the ceramide quantification method. (A) Study design. The samples for ceramide analysis were obtained from the "omics" dissection groups of the two studies. (B) Ceramide quantification method.

Selection and establishment of ceramide panel

The results from initial development experiments informed the selection of the four ceramides for the assay (Cer(d18:1/16:0), Cer(d18:1/18:0), Cer(d18:1/24:0), and Cer(d18:1/24:1)).

Initially, we evaluated the overall ceramide profiles of mouse lungs and plasma by high-resolution mass spectrometry with a Thermo Q-Exactive instrument (Waltham, MA, USA). Data-independent LC–MS/MS acquisition was performed with an inclusion list of all possible molecular masses of ceramides with different sphingoid bases, including d18:0, d18:1, and d18:2, as well as different combinations of fatty acids (Supplementary Table S1). Guided by data from literature on ceramide fragmentation [39], we identified the main endogenous profiles of ceramides, including those of Cer(d18:0/24:1), Cer(d18:0/16:0), Cer(d18:0/24:0), Cer(d18:0/22:0), Cer(d18:1/16:0), Cer (d18:1/18:0), Cer(d18:1/20:0), Cer(d18:1/22:0), Cer(d18:1/22:1), Cer(d18:1/23:0),Cer(d18:1/23:1), Cer(d18:1/24:0), Cer(d18:1/24:1), Cer(d18:1/25:0), Cer(d18:1/26:0), Cer(d18:2/20:0), Cer(d18:2/22:0), Cer(d18:2/23:0), Cer(d18:2/24:0),and Cer(d18:2/24:1) (Supplementary Figure S2).

As we aimed to develop a robust method that would support high-throughput analyses of large sample sets of preclinical and, potentially, clinical studies, we guided our final method selection by the requirements of the global initiative for harmonization and standardization, including stringent validation requirements [40]. Considering the heterogeneity of the endogenous profile, only a few standards (light- and heavy-isotope-labeled) were commercially available, such as those for Cer(d18:1/16:0), Cer(d18:1/18:0), Cer(d18:1/24:0), and Cer(d18:1/24:1). For these compounds, we created a targeted absolute quantification MRM-based method by using an 8060 triple quadrupole mass spectrometer from Shimadzu (Reinach, Switzerland).

Initially, we included the other endogenous ceramides, for which standards were lacking, in a relative quantification method, normalizing to the intensity of Cer(d18:0-d7/16:0) or Cer(d18:0-d7/24:0) depending on their elution time. However, this relative quantification method demonstrated poor performance when tested with reference QC plasma over 6 days, with CVs of more than 40%. Therefore, for our studies, we focused on the robust, fully quantitative method for Cer(d18:1/16:0), Cer(d18:1/18:0), Cer(d18:1/24:0), and Cer(d18:1/24:1) rather than a larger ceramide panel. Of note, this observation is in line with a published more comprehensive comparative study between targeted and non-targeted lipidomics, which showed that the overall CV performance for

untargeted methods can vary between 30% to 200% making it inappropriate for detection of minor changes [41].

Tissue processing for the ceramide panel

Samples were processed as several randomized batches. Frozen tissue slices from the left lung lobe and liver tissue were homogenized in 150 mM ammonium bicarbonate by using a bead-assisted procedure in a Tissue Lyser II (Qiagen, Hilden, Germany). Stainless steel beads (2.8 mm; LabGene, Châtel-Saint-Denis Switzerland) were added to each tube, and the samples were processed over two cycles at 30 Hz for 2 min per cycle. The abdominal aortic arch was homogenized in 150 mM ammonium bicarbonate by using a Branson W4500 instrument (Bransons Ultrasonics, CT, USA). The tissue was fully homogenized over two runs of 20 s at an amplitude of 20%. Aliquots of tissue homogenate were centrifuged for 5 min at 13,000 rpm in an Eppendorf centrifuge (Vaudaux-Eppendorf AG, Schönenbuch, Switzerland), and protein concentrations were determined by the Bradford assay.

Sample processing for the ceramide panel

We chose a chloroform-free lipid extraction method based on the use of butanol/methanol and heptane/ethyl acetate, as it provides a safer alternative to the Bligh and Dyer [42] and MTBE [43] protocols and allows highly efficient extraction of all major lipid classes and across diverse sample matrices [37, 38]. Ceramides were extracted from tissue and plasma samples by using an adjusted two-phase BUME extraction method [37, 38]. Each batch of samples (maximum 30 samples) included a blank sample, an internal standard (IS) blank sample, seven levels of calibration standards, the study samples, and three quality controls (QC). Ceramide-free SigMatrix serum diluent was used as a matrix for blank samples and calibrants. The highest level of the calibration curve (SS7) ceramide LIPIDOMIX® Mass Spec Standard solution was initially diluted 10-fold in 1:1 dichloromethane/methanol. Further serial dilutions of SS7 were prepared with methanol. The calibration ranges covered: 0.02–3 μM for Cer(d18:0/16:0); 0.01–1.5 μM for Cer(d18:0/18:0); 0.05–7.5 μM for Cer(d18:0/24:0); and 0.025–3.75 μM for Cer(d18:0/24:1(15Z)). The IS working solution was prepared from Deuterated Ceramide LIPIDOMIX® Mass Spec Standard by diluting the stock solution 100 times with 1:1 dichloromethane/methanol. All samples were spiked with 10 μL of IS solution, while seven calibrant samples were additionally spiked with diluted standard solutions. The processed sample volume varied from 2 to 100 μL across the sample types and was adjusted on the basis of total protein concentration.

For lipid extraction, the samples were treated with 300 μL of cold (-20°C) 3:1 butanol/methanol mixture to facilitate protein precipitation and then vortexed for 10 min at 2000 rpm at room temperature. The samples were then vortexed with 300 μL of 3:1 heptane/ethyl acetate for 10 min at 2000 rpm. Addition of 300 μL of acetic acid led to the formation of two phases. After mixing for 5 min at 2000 rpm, the samples were centrifuged for 5 min at 5000 rpm to achieve full separation of the two phases. The upper layer (360 μL) was transferred to 2-mL self-lock Eppendorf collection tubes. The residual samples were treated again with 320 μL of heptane/ethyl acetate and then mixed and centrifuged as described before. The upper layer thus obtained (320 μL) was combined with the first fraction in the collection tubes. Finally, the samples were re-extracted with 250 μL of heptane/ethyl acetate, and, after mixing and centrifugation, the last 250 μL of the upper layer was combined with the two previous collections. The solution in the collection tubes was dried in a vacuum concentrator (Christ, Osterode am Harz, Germany). The dried samples were suspended with 300 μL of 7.5 mM ammonium acetate in 2-propanol/methanol/chloroform (4:2:1). After centrifugation at 4°C and 12,700 rpm for 10 min, 100-μL aliquots were transferred to plastic tubes and analyzed.

UPLC–MS analysis for ceramide panel

Targeted LC–MS analysis was performed with a Nexera UPLC system coupled with an 8060 triple quadrupole mass spectrometer from Shimadzu (Shimadzu Schweiz, Reinach, Switzerland) in MRM mode. Individual ceramide standard solutions were used to select the optimal transition and source settings. The electrospray ionization source was set to nebulizing gas flow of 2 L/min, heat gas flow of 10 L/min, interface temperature of 300℃, DL temperature of 200℃, heat block temperature of 250℃, and drying gas flow of 10 L/min.

The samples were separated on an ACQUITY BEH C18 2.1-mm × 100-mm column (Waters, Eschborn, Germany) heated up to 60℃ during the runs. The mobile phase was based on solvent A (0.1% formic acid in water) and solvent B (4:3 acetonitrile/2-propanol). The gradient elution program was as follows: delivering 85% of B during the first 0.5 min; ramping from 85% to 100% between 0.5 and 1.5 min; holding at 100% from 1.5 to 4.1 min; and set back to 85% B at 4.1 min, followed by equilibration during last 1.2 min. The total run time was 5.3 min, with a flow rate of 0.5 mL/min. To reduce carry over, an external wash program with R_0 (2-propanol/methanol/acetonitrile/water [1:1:1:1]) and R_3 (2-propanol) was used before and after aspiration. The optimized MS settings for MRM are specified in Table 1.

Table 1. Acquisition settings for targeted ceramide analysis. Two ions were monitored for the ceramides: the quantifier (in bold) ion is an 18:1 fatty acid fragment, and the qualifier is a water-loss fragment.

Target	Precursor (m/z)	Product (m/z)	Q1 (V)	CE	Q3 (V)
d18:1/16:0	**538.50**	**264.30**	**-20**	**-29**	**-27**
d18:1/16:0	538.50	520.45	-20	-15	-24
d18:1/18:0	**566.50**	**264.35**	**-20**	**-26**	**-27**
d18:1/18:0	566.50	548.45	-20	-14	-26
d18:1/24:0	**650.50**	**264.25**	**-24**	**-32**	**-20**
d18:1/24:0	650.50	632.55	-32	-16	-30
d18:1/24:1	**648.55**	**264.35**	**-24**	**-30**	**-27**
d18:1/24:1	648.55	630.35	-24	-17	-30
d18:1/16:0 D7	**545.20**	**271.30**	**-28**	**-25**	**-15**
d18:1/18:0 D7	**573.40**	**271.30**	**-28**	**-29**	**-16**
d18:1/24:0 D7	**657.50**	**271.30**	**-38**	**-30**	**-18**
d18:1/24:1 D7	**655.55**	**271.30**	**-36**	**-32**	**-16**

MS data were processed by using LabSolutions 5.93, and csv data files were generated and subjected to statistical processing.

Method validation of the ceramide panel

The main method performance parameters were assessed during method validation for targeted quantification of four ceramides in human plasma. The main tests included: selectivity of the analysis, linearity of response function (calibration curves), lower limit of detection (LOD), lower limit of quantification (LLOQ), upper limit of quantification (ULOQ), upper working range limit (UWRL), lower working range limit (LWRL), bias, repeatability of the method, intermediate precision, instrumental repeatability, stability of the standards, stability of sample extracts, and stability of plasma.

Selectivity. The selectivity of IS compounds was evaluated by injecting blanks and lipid extracts with and without IS. The acceptance criteria were: concentration of analyte in the solvent less than 20% relative to the first calibration level signal; area/response for the residual response of the blank less than 5% relative to the signal of IS; and quantifier/qualifier response ratio in the matrix within ±25% of the qualifier ratio in the calibration standards.

Assessment of response function. Seven calibration levels (Table 2) were processed through sample preparation and injected (3 injections per each level) over 5 days by two independent operators. Response function was assessed by linear regression analysis. The acceptance criteria were: no bias for residuals plots; coefficient of determination R^2 higher than 0.97; and deviation of determined concentration from calculated concentration within ±20% for the lowest level and

within ±15% for other calibration levels. Of the seven levels, at least five had to fulfil these criteria, including those of the lowest and highest levels.

Table 2. Ranges of concentration evaluated during validation**.

Compound	STD7, mM/L	STD6, mM/L	STD5, mM/L	STD4, mM/L	STD3, mM/L	STD2, mM/L	STD1, mM/L	Regression model
d18:1/16:0	3	1	0.5	0.2	0.1	0.05	0.02	Linear
d18:1/18:0	1.5	0.5	0.25	0.1	0.05	0.025	0.01	Linear
d18:1/24:0	7.5	2.5	1.25	0.5	0.25	0.125	0.08	Linear
d18:1/24:1	3.75	1.25	0.625	0.25	0.125	0.0625	0.025	Linear

**The current concentration represents not the actual concentration of the compound in final aliquot but the recalculated concentration in the plasma sample.

LOD/LOQ. LOD was determined as 3 * SD_{stdl}, where SD_{stdl} is the standard deviation (SD) of the lowest standard concentration level under intermediate precision conditions (18 series in triplicate), including two operators. LLOQ is the concentration above which the analyte was reliably quantified with suitable precision and accuracy. LLOQ was calculated as 10 * SD_{stdl}. ULOQ is the highest concentration below which the analyte was quantified with suitable precision and accuracy.

Analytical accuracy, repeatability, and intermediate precision. These parameters were assessed by preparing the next series of samples: intact plasma sample, diluted plasma (1/2, 1/5, 1/10, 1/25, and 1/50), and plasma samples spiked with the concentrations of compounds equal to calibration levels 3, 4, and 5. Sample extraction was performed over five independent preparations in triplicates and by two different operators using three different UPLC columns. The working range was defined as the range where measurements were accurate and precise for a given matrix; it was determined by the lower and upper limits of the working range (the lowest and highest concentrations, respectively, for which the tolerance interval of accuracy was within the acceptance threshold). The acceptance criteria included: recovery within ±20% for the lowest level and within ±15% for the rest; a β-tolerance of 95% as the coverage factor for plotting accuracy profiles [44]; and acceptance limits (total error comprising bias and precision per level of concentration) of ±35%.

Instrument repeatability. Instrument repeatability was accessed by repeated injection (10 times) of calibration level 4 solution.

Robustness. Robustness was checked by evaluating the impact of varying the extraction conditions in the first two steps in six replicates. The maximum difference had to be less than 15% and at least four of the six replicates had to fulfill the criteria.

Repeatability and intermediate precision of the method was accessed during five days in triplicate.

Stability test. Within the scope of the stability test, the stability of the calibration/IS as tested during 1 month during 1 month of storage at -20°C. The stability of plasma was assessed at -80°C, +4°C, and bench conditions, and the stability of the lipid extracts was tested at -20°C. The stability of plasma was also tested after three freeze (-80°C)–thaw cycles. The stability of the final extract in the injector was tested under refrigeration and up to 8°C.

QC procedure for ceramide panel

A QC procedure was established to ensure the robustness of MS analysis. For this purpose, commercial female mouse plasma was ordered from Seralab, and the endogenous levels of ceramides were determined over 5 days in 15 identical aliquots per batch (total of five batches). The data evaluation pipeline was created as a Shiny web application by using the R statistical software package [45]. The average concentration and SD for five batches were calculated for each compound. The acceptance range was set as average ± 3SD. Each batch of mouse tissue/plasma samples included several QC samples (one QC sample per every ten unknowns). The QC samples

were prepared identically to the unknowns and equally distributed in the injection sequence. The QC data were plotted against the reference set from the database (see Supplementary Figure S5). The batch was considered acceptable only if ≥70% of the QC samples were in the acceptance range for each compound.

Statistical analysis

For tissue analyses, the concentration data were normalized to the total protein concentration measured by the Bradford assay. A linear model was fitted for each exposure condition and the corresponding control group, and p values from a t-statistic of log-transformed data were calculated. The Benjamini–Hochberg method was used to adjust for multiple testing effects. Ceramides (or their derived fractions and ratios) with adjusted p values <0.05 were considered differentially abundant.

Method automation

To support the routine use of the established method, we implemented an automated version of the BUME extraction using a Tecan Evo Freedom 200 liquid handler robot (Männedorf, Switzerland). The Tecan Evo workspace layout required to perform the extraction is shown in Figure 1A. Generally, all the extraction steps were implemented in correspondence with the manual procedure (Figure 2B). However, minor adjustments were necessary for mixing and centrifugation, because the internal shaker of the robot had a maximum shaking speed of 1000 rpm and, for centrifugation performed with an external centrifuge, the 96-well deep-well rotor speed limit was 4000 rpm. Of note, dispatching of IS was especially optimized, because the dichloromethane/methanol (1:1) solvent mixture was prone to dripping. For this, an air gap was added, the aspiration/dispensing speed was adjusted, and single-channel dispensing into the solution was implemented. As a result, inter-assay CVs of approximately 5% were achieved on the full 96-well plate. In addition, we compared the performance of the manual and automatized protocol using NIST reference plasma. The results obtained with the automatized protocol were in the acceptance range of validation requirements (Supplementary Table S2).

Journal Pre-proof

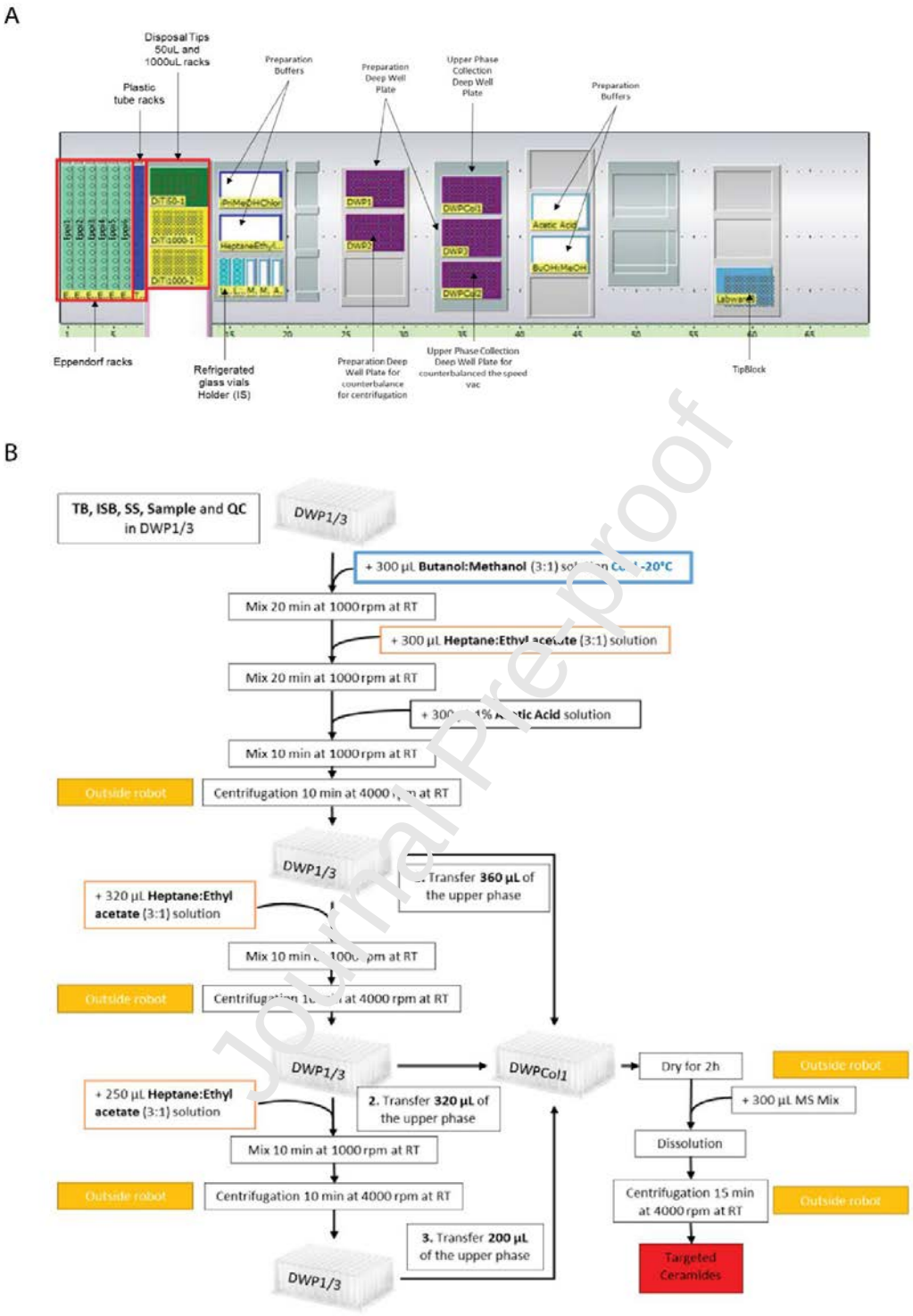

*Fi*gure 2. 96-well plate BUME extraction assisted by Tecan Freedom Evo 200 robot. (a) Robot workspace layout; (b) Schematic representation of the main steps performed by robotic script.

Gene expression analysis

Total RNA was isolated by using the miRNeasy Mini Kit (Qiagen, Hilden, Germany) and quality-checked by using an Agilent 2100 Bioanalyzer (Agilent Technologies, Santa Clara, CA, USA)

as described previously [33]. RNA (100 ng) was reverse-transcribed, amplified, purified, and hybridized onto MG430 2.0 GeneChips (Affymetrix, Santa Clara, CA, USA) and evaluated by standard procedures [35, 36].

For statistical analysis, a linear model was fitted for each exposure condition and the respective sham group. p values were calculated from moderated t-statistics with the empirical Bayes approach [46]. Genes with Benjamini–Hochberg (FDR)-adjusted p values <0.05 were considered differentially expressed.

Here, we only focus on ceramide-related gene changes. Broader analyses of the observed gene expression changes are reported elsewhere (Titz et al., submitted, [34]).

Protein expression analysis

Proteome changes were assessed by isobaric tag-based quantification by using the iTRAQ® approach as described previously [5]. Briefly, frozen tissue was homogenized in tissue lysis buffer (BioRad Laboratories, Hercules, CA, USA) before acetone precipitation. Protein precipitates were resuspended and processed by the iTRAQ 8-plex labeling procedure in accordance with the manufacturer's instructions (AB Sciex, Framingham, MA, USA).

Multiplexed samples were purified and analyzed in random order by using an Easy nanoLC 1000 instrument equipped with a 50-cm Acclaim™ PepMap™ 100 C18 LC column (2-µm particle size, both Thermo Fisher Scientific, Waltham, MA, USA) connected online to a Q Exactive mass analyzer (Thermo Fisher Scientific, Waltham, MA, USA). Each sample was injected twice into the same column with two different analytical methods—one fast and another sensitive—as previously described [47]. The outputs of both MS runs were combined as merged mass lists and interrogated against the mouse reference proteome set (UniProt, canonical isoforms only) by using Proteome Discoverer version 1.4 (Thermo Fisher Scientific, Waltham, MA, USA). The SequestHT program in Proteome Discoverer was used as the search tool, and iTRAQ reporter-ion intensities were determined from Proteome Discoverer. The Percolator node of Proteome Discoverer was used to estimate peptide-level FDR-adjusted p values (q-values).

iTRAQ peptide-level quantification data were exported and further processed in the R statistical environment [45]. Quantification data were filtered for q-values <0.01 and "unique" quantification results, as defined by Proteome Discoverer. A global variance-stabilizing normalization was performed with the corresponding Bioconductor package in R [48, 49]. Each iTRAQ reporter-ion set was normalized to its median, and protein expression values were calculated as the medians of these normalized peptide-level quantification values [50].

For statistical analysis, a linear model was fitted for each exposure condition and the respective sham group. p values were calculated from moderated t-statistics with the empirical Bayes approach [46]. Proteins with Benjamini–Hochberg (FDR)-adjusted p values <0.05 were considered differentially expressed.

Here, we only focus on ceramide-related protein changes. Broader analyses of the observed protein expression changes are reported elsewhere (Titz et al., submitted, [34]).

Data availability

Ceramide lipidomics datasets are available as a Supplementary Data file.

3. Results

2.1. Method establishment and validation

To establish a ceramide assay of sufficient accuracy and precision for comparative animal studies and clinical investigations, we developed and validated—using human plasma—an absolute LC–MS/MS quantification method for a panel of four ceramides: Cer(d18:1/16:0), Cer(d18:1/18:0), Cer(d18:1/24:0), and Cer(d18:1/24:1 (15Z)). Our decision to select this ceramide panel was prompted by their suggested clinical relevance as risk factors for cardiovascular diseases

and COPD [51, 52], the observation that, in mice, CS affects the lung concentrations of ceramides with different chain lengths (see introduction, [13]), as well as our initial method development results and the availability of ceramide standards (see Materials and Methods).

We developed a method based on butanol–methanol (BUME) extraction and LC separation on a C_{18} reverse-phase column. Figure 3A shows the separation efficiency of the four ceramides during the short 5-min elution program of the established LC–MS/MS method. The ceramides were quantified by electrospray ionization in positive ion mode, which allowed us to observe the specific multiple reaction monitoring (MRM) transitions from the ceramide parent ions $[M+H]^+$ to their sphingosine fragments (*m/z* of 264 and 271 for standards and IS, respectively). The second transition between parent ion and water loss $[M-H_2O+H]^+$ fragment was monitored as the qualifier ion. The method provided selective baseline separation of targets and deuterated IS in the matrix, with the matching retention time of targets versus deuterated analogs providing additional evidence for confident identification of the targets.

We validated the established method by following the recommendations of the US Pharmacopeia and National Formulary (USP40/NF35, 2017), ICH Harmonized Tripartite Guideline, Validation of Analytical Procedures: Text and Methodology Q2 (R1) [53], and Bioanalytical Method Validation, Guidance for Industry from May 2018 [54].

In collaboration with Avanti Polar Lipids (Alabaster, AL, USA), we established premixed solutions of standards (Ceramide LIPIDOMIX® Mass Spec Standard and Deuterated Ceramide LIPIDOMIX® Mass Spec Standard), for which each compound concentration was adjusted on the basis of its endogenous concentration in human plasma. The Ceramide LIPIDOMIX® Mass Spec Standard was used to prepare calibration curves, and the Deuterated Ceramide LIPIDOMIX® Mass Spec Standard was added as an IS mixture to all samples. Quantification was performed by using seven-level calibration curves for each ceramide injected in duplicate. The calibration concentration ranges were specifically adapted to cover the more abundant Cer(d18:1/24:1(15Z)) and Cer(d18:1/24:0) ceramides as well as the less abundant Cer(d18:1/16:0) and Cer(d18:1/18:0) ceramides in plasma. Figure 3D shows the overall performance of the calibration curves for all compounds during the whole validation process. The coefficient of determination (R^2) for the linear regression (1/x weighted) models was higher than 0.99, with equivalent distribution of the relative residuals. As expected, the computed concentrations were spread around the target values, and no clear curvature was observed.

The main method performance metrics obtained during method validation are summarized in Table 3. The working range (i.e., the range in which quantification of endogenous compounds is accurate and precise) was defined between the LWRL and UWLR. These values were obtained by an accuracy profile test, for which the measured concentrations of ceramide targets at different concentrations (spiked and diluted matrices) were compared with the expected/theoretical concentrations. Figure 3C represents the accuracy profile for Cer(d18:1/24:1(15Z)) measured for nine plasma concentrations. As an acceptance criterion, we required the difference between the measured and theoretical values to be in the range of ±35% (Figure 3B). The lowest and highest concentrations fulfilling this criterion were defined as the LWRL and UWLR, respectively (see Supplementary Figures S3 and S4 for the accuracy profiles of other targets). More details on the validation procedure are available in the supplementary material (Supplementary Tables S2-S21).

Table 3. Detection range of ceramides and the main validation results for human plasma.

Target	d18:1/16:0	d18:1/18:0	d18:1/24:0	d18:1/24:1(15Z)
LOD, pmol/µL	0.007	0.005	0.025	0.009
LLOQ, pmol/µL	0.025	0.017	0.084	0.030
LWRL, pmol/µL	0.064	0.017	1.3	0.030
UWLR, pmol/µL	3.000	0.325	7.500	3.750
ULOQ, pmol/µL	3.000	1.500	7.500	3.750
Accuracy, %relative	-11 to 8	-3 to 5	-1 to 2	-1 to 12

error				
Precision of the analytical method *, CV%	Intra-run: 1–6 Inter-run: 5–7	Intra-run: 0–10 Inter-run: 8–12	Intra-run: 4–9 Inter-run: 5–10	Intra-run: 0–6 Inter-run: 3–9
Precision of the whole process (plasma)	Nominal concentration: 0.231 pmol/µL Intra-run: 7% Inter-run: 14%	Nominal concentration: 0.113 pmol/µL Intra-run: 9% Inter-run: 14%	Nominal concentration: 2.855 pmol/µL Intra-run: 5% Inter-run: 12%	Nominal concentration: 0.992 pmol/µL Intra-run: 6% Inter-run: 8%

*The range shows the minimum and maximum deviation in % within different concentration levels; LOD – lower limit of detection, LLOQ – lower limit of quantification, LWRL –lower working range limit, UWLR – upper working range limit, ULOQ – upper limit of quantification.

Overall, the quantification was linear for Cer(d18:1/16:0) in the range of 0.025–3 pmol/µL; Cer (d18:1/18:0), 0.017–1.5 pmol/µL; Cer(d18:1/24:0), 0.084–7.5 pmol/µL; and Cer(d18:1/24:1(15Z)), 0.03–3.75 pmol/µL. The working range in plasma (defined between LWRL and UWLR; Table 3) for Cer(d18:1/16:0) was between 0.064–3 pmol/µL; Cer(d18:1/18:0), 0.017–0.323 pmol/µL; Cer(d18:1/24:0), 1.3–7.5 pmol/µL; and Cer(d18:1/24:1(15Z)), 0.03–3.75 pmol/µL. The nominal plasma concentrations (Table 3) of all four ceramides were aligned with reported ranges for healthy individuals [55].

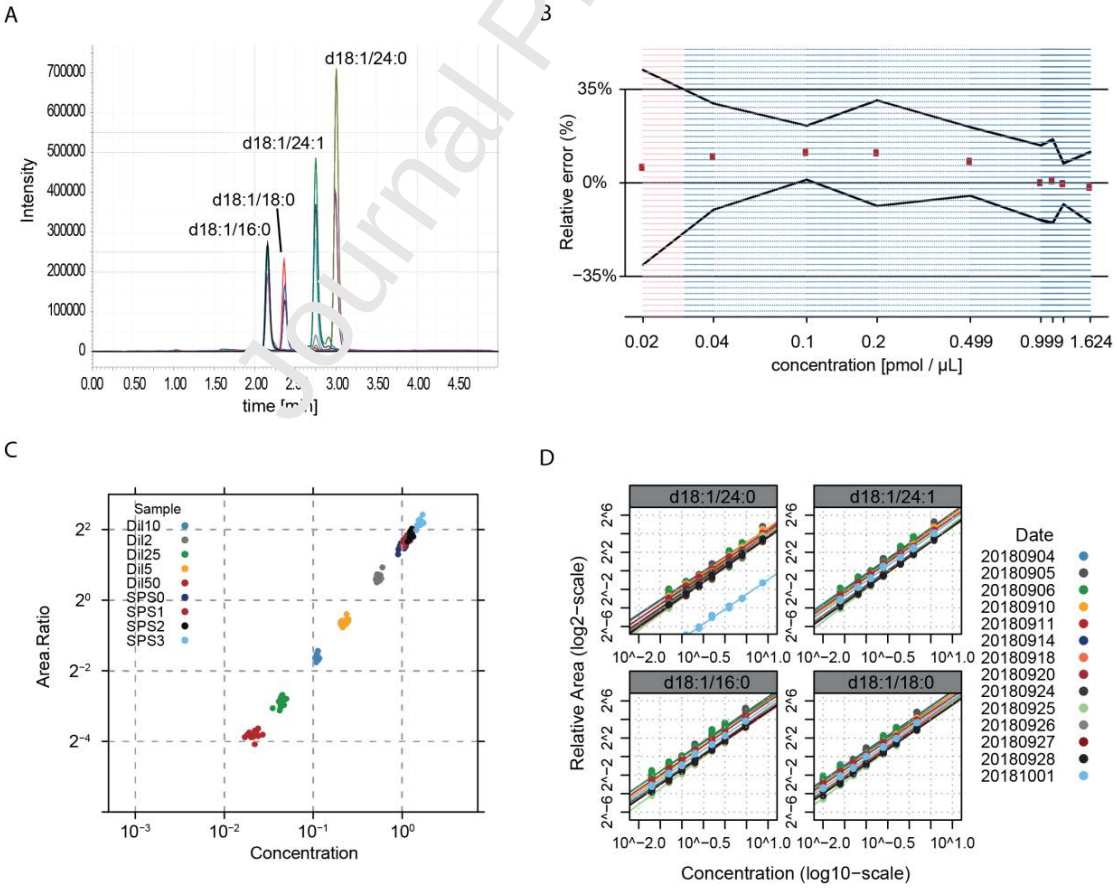

Figure 3. Method performance. (a) UPLC–MS/MS chromatogram of four ceramides and labeled internal standards. (b) Example for identification of the LLOQ from the accuracy profile of Cer(d18:1/24:1(15Z)). (c) Overlay of accuracy profile area ratio responses for Cer (d18:1/24/1(15Z)) on different days corresponding to lipid extracts at different concentration levels, resulting in an increase in peak area response at specific m/z values and retention times. (D) Precision (repeatability and intermediate precision) over 14 independent days of the calibration curves by using a linear regression model with a weighting factor of 1/x.

Short-term stability assessment results showed that ceramide standards stored at -20°C were stable for at least 1 month (long-term stability was not assessed). Re-suspended final extracts were stable in the injector at +8°C for up to 72 h. Lipids extracts stored at -20°C were stable for up to 1 week. Plasma samples were stable at room temperature on the bench for up to 2 days and at -80°C for at least for 1 month (long-term stability was not assessed.). Analytes were stable in plasma after three freeze/thaw cycles (-80°C). Additional stability data are available in the supplementary material (Supplementary Tables S16–S21).

To ensure the robustness of the established assay during study analyses, we also established a quality control (QC) procedure. A QC evaluation tool was created as a Shiny web application by using the R statistical software package [45]. Reference ranges were established for mouse plasma over 5 days in 15 identical aliquots per batch (total of five batches). The acceptance range was set as average ± 3SD. For study batches, one freshly prepared mouse plasma QC sample was included per every ten unknowns. A batch was considered acceptable only if ≥70% of the QC samples were in the acceptance range for each compound.

Furthermore, to support the routine use of the established method, we implemented an automated version of the BUME extraction using a Tecan Evo Freedom 200 liquid handler robot (Männedorf, Switzerland). With this automated procedure, we achieved inter-assay coefficients of variation (CVs) of approximately 5% on the full 96-well plate (Supplementary Table S22).

In summary, the established method is sensitive, accurate, and sufficiently precise for quantifying all four endogenous ceramides in plasma and different tissue samples. This fully clinically compliant method, with either manual or fully automatized sample preparation, has an overall analysis time of 5.5 min per sample and supports a daily throughput of up to 200 samples.

2.2. Effect of CS and potential MRTP aerosols on ceramide profiles in the lungs of ApoE$^{-/-}$ mice

In two independent 6-month inhalation toxicology studies in ApoE$^{-/-}$ mice, we evaluated how exposure to potential MRTP aerosols affected the established four-ceramide panel relative to the positive control (3R4F CS exposure; Figure 4). The ApoE$^{-/-}$ HnB study [33] assessed the effects of two heat-not-burn tobacco products (THS 2.2 and CHTP 1.2) relative to 3R4F CS and, additionally, the effects of cessation and switching to CHTP 1.2 aerosol after 3 months of 3R4F CS exposure. The ApoE$^{-/-}$ e-vapor study assessed e-vapor formulations of PG and VG, nicotine (N), and flavors (F). To this end, in addition to sham (control; fresh air exposure) and 3R4F CS exposure, this study included exposure to aerosolized CARRIER, BASE, and TEST liquids [34]. Importantly, in each study, the nicotine concentrations were matched between 3R4F CS and the nicotine-containing potential MRTP aerosols (Table 4). A detailed exposure characterization is presented in [33] and [34].

At the 3- and 6-month time points, the levels of the four ceramides were quantified in nine (ApoE$^{-/-}$ HnB study) or ten (ApoE$^{-/-}$ e-vapor study) biological replicates per group. The ceramide concentrations were normalized to protein levels for solid tissues and to volume for plasma/serum. In addition, as ceramide ratios have been found to be relevant in previous studies [13], we also computed the six ratios between the four measured ceramides as well as the ceramide fractions (as the concentration of a given ceramide over the total concentration of the four-ceramide panel).

In lung tissues from both ApoE$^{-/-}$ studies, Cer(d18:1/16:0), Cer(d18:1/24:0), and Cer(d18:1/24:1(15Z)) were present at almost similar concentrations, while Cer(d18:1/18:0) was

approximately at a level of 3–5% relative to the total ceramide level (Supplementary Figures S6 and S7).

In relation to individual ceramide measurements, in the ApoE$^{-/-}$ HnB study, only Cer(d18:1/18:0) was significantly decreased in the 3R4F group relative to the sham group (Figure 4A); in the ApoE$^{-/-}$ e-vapor study, only Cer(d18:1/24:1(15Z)) was significantly increased in the 3R4F group relative to the sham group (Figure 4C). In terms of the calculated ceramide fractions, the Cer(d18:1/18:0) fraction demonstrated a consistent decrease upon 3R4F CS exposure in both studies.

The calculated ceramide ratios showed the most robust 3R4F CS exposure responses, indicating an opposing effect of 3R4F CS exposure on long-chain (C16 and C18 fatty acids) versus very-long-chain (C24 fatty acids) ceramides. In both ApoE$^{-/-}$ studies, 3R4F CS groups showed a consistent increase (relative to the sham groups) in ratio between ceramides with a 24:0 or 24:1 fatty acid chain versus Cer(d18:1/18:0) and a decrease in the Cer(d18:1/18:0) to Cer(d18:1/16:0) ratio (Figure 4A and C). Figure 4B and D illustrate the clear shift in these ratio distributions for the 3R4F CS groups.

Unlike 3R4F CS exposure, THS 2.2, CHTP 1.2, and e-vapor aerosol exposure only had limited (non-significant) effects on the four-ceramide panel in the lungs. At the 6-month time point, in the ApoE$^{-/-}$ HnB study, the effects of both cessation and switching to CHTP 1.2 were much reduced relative to 3R4F CS exposure (Figure 4A), with three long- to short/medium-chain ratios and the Cer(d18:1/18:0) fraction reaching significance for switching versus sham.

Journal Pre-proof

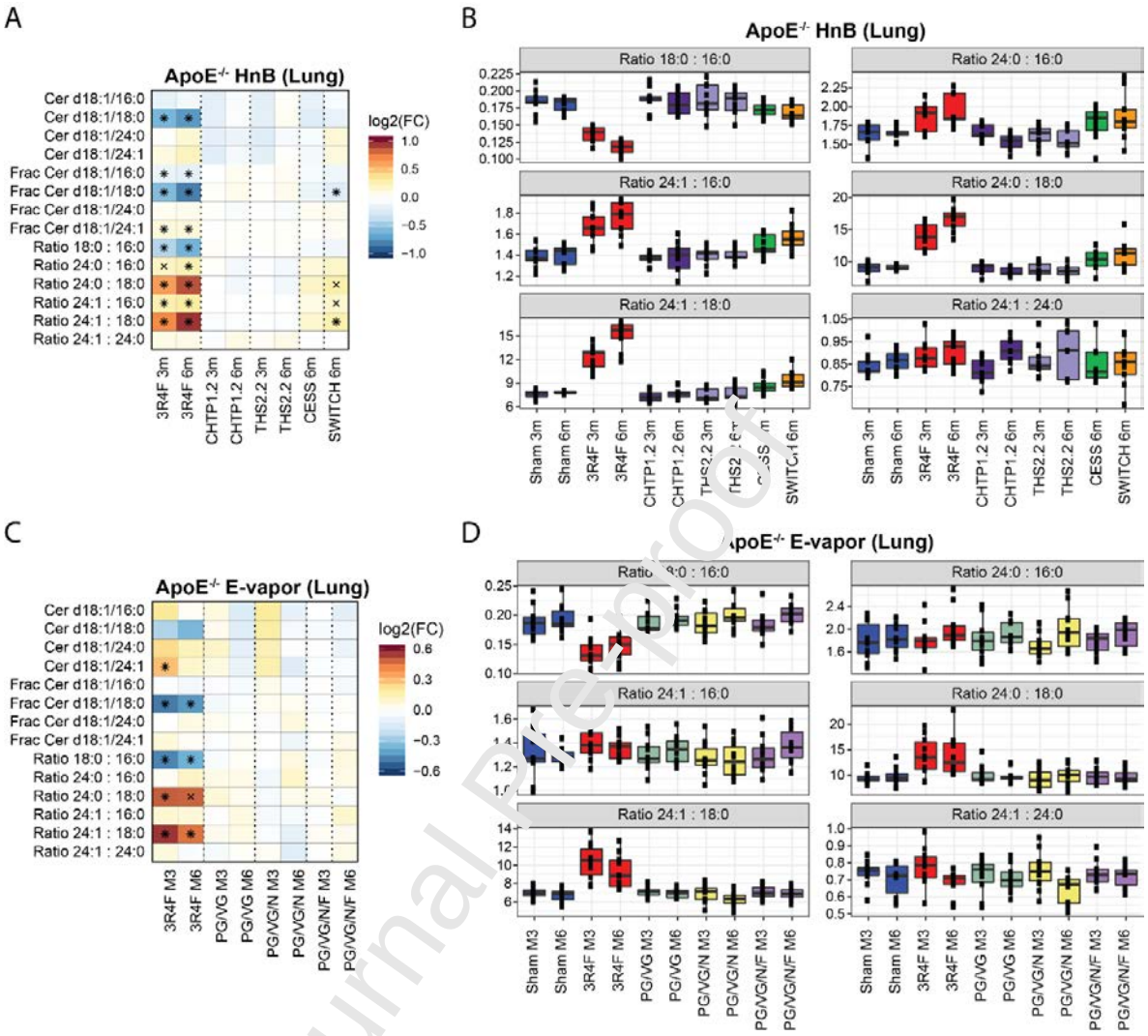

Figure 4. Effects of CS and potential MRTP aerosols on lung ceramide profiles in two ApoE$^{-/-}$ mouse inhalation studies. (a) Concentration profiles of ceramide, relative fractions of ceramides (Frac), and ceramide ratios in the lungs in the ApoE$^{-/-}$ HnB study. Fold changes relative to the respective sham group are color-coded, and statistical significance is marked (FDR-adjusted p values: ×<0.05 and *<0.01). If applicable, missing values are indicated in grey. (b) Boxplots of ceramide ratios in the lungs in the ApoE$^{-/-}$ HnB study. (c) Same as panel A, but for the ApoE$^{-/-}$ e-vapor study. (d) Same as panel B, but for the ApoE$^{-/-}$ e-vapor study.

2.3 Effect of CS and potential MRTP aerosols on ceramide profiles in other tissues in ApoE$^{-/-}$ mice

In addition to the lungs, we also analyzed the four-ceramide panel in plasma and, for the ApoE$^{-/-}$ HnB study, in the serum, liver, and abdominal aorta (Supplementary Figure S8). In the ApoE$^{-/-}$ HnB study, the effects of 3R4F CS exposure in serum and plasma were similar to those in the lungs, including a prominent decrease in the Cer(d18:1/18:0) fraction and increase in the ratios of 24:1 and 24:0 to 18:0 (Supplementary Figure S8 A). While these ceramide measurements all showed a similar trend in plasma samples in the ApoE$^{-/-}$ e-vapor study, only the Cer(d18:1/24:1(15Z)) to Cer(d18:1/18:0) ratio reached significance for 3 months of 3R4F exposure (Supplementary Figure S8 B). In contrast, in both ApoE$^{-/-}$ studies, no significant effects were observed in the HnB and e-vapor product aerosols exposure groups.

In the ApoE$^{-/-}$ HnB study, the four-ceramide panel also showed a similar exposure response to 3R4F CS in liver. However, similar to the response observed in plasma in this study, the effects were stronger and only reached significance at the 6-month time point. The 3R4F CS group showed an especially strong effect on the 24:1 to 18:0 ceramide ratio in the liver, whereas none of the other exposure groups demonstrated a significant effect on the ceramide profiles in this tissue. Finally, in the abdominal aorta, 3R4F CS exposure caused a significant increase in the 24:1 to 18:0 ceramide ratio relative to sham exposure only at the 3-month time point (Supplementary Figure S8 B).

In addition to the differences in ceramide ratios among the groups, the differences in the baseline levels of the four measured ceramides among the tissues were also noteworthy in the ApoE$^{-/-}$ HnB study (Supplementary Figure 6): A substantial shift in the relative distribution of the ceramides species was detected, with an overall increase in the fraction of Cer(d18:1/18:0) from a small percentage in plasma/serum/lungs to up to more than 10% in the abdominal aorta.

2.4 Ceramide metabolism-related gene and protein expression changes

To evaluate the molecular context of the observed ceramide changes, we investigated the changes in gene and protein expression in ceramide metabolism pathways in both studies.

On the protein level, a strong and consistent upregulation of Asah1 was observed in the lungs upon 3R4F CS exposure in both ApoE$^{-/-}$ mouse studies (Figure 5A and B). The main biochemical function of Asah1 is to hydrolyze lysosomal membrane ceramides into sphingosine, the backbone of all sphingolipids, to regulate many cellular processes. We had also observed upregulation of Asah1 in the lungs upon CS exposure in our previous study in ApoE$^{-/-}$ mice, which motivated us to further investigate ceramide ratios in the present study [13]. Of note, on an individual animal level, our findings revealed a strong association between the 24:1 to 18:0 ratio and Asah1 expression level (Figure 5C and D).

Additionally, a strong upregulation of glucocerebrosidase (Gba was observed in response to CS exposure in both studies (Figure 5A and B). Gba breaks down the glycolipid glucocerebroside into glucose and ceramide inside lysosomes [56].

Other ceramide pathway enzymes such as alkaline ceramidase 2 (Acer2) and ceramide synthase 4 (Cers4), were significantly downregulated in the lungs upon CS exposure in the ApoE$^{-/-}$ HnB study (Figure 5A); however, they only demonstrated a downward trend in the ApoE$^{-/-}$ e-vapor study (Figure 5B). Acer2 is localized in the Golgi complex and hydrolyzes ceramides to sphingosine and sphingosine phosphate. This enzyme plays a key role in maintaining the balance of sphingosine phosphate (S1P) and its dehydro-precursor form in plasma by controlling the generation of the sphingosine (SPH) bases and dihydrosphingosine (dhSPH) in hematopoietic cells [57]. Of note, on an individual animal level, there was a negative association between the 24:1 to 18:0 ratio and Acer2 expression level (Figure 5C and D). Cers4 is one of the six ceramide synthase enzymes and is specifically responsible for the production of C18–C20 ceramides from sphingosine and dedicated fatty acids in the endoplasmic reticulum (ER) [58].

In the liver, ceramide kinase (Cerk) was significantly downregulated upon 3R4F CS exposure (Supplementary Figure S9) in the ApoE$^{-/-}$ HnB study and demonstrated a downward trend in the ApoE$^{-/-}$ e-vapor study. Cerk is the only enzyme known to be responsible for the production of ceramide phosphate from ceramide [59] and prefers ceramide species with acyl chains longer than 12 carbons [60].

In contrast to 3R4F CS exposure, exposure to potential e-vapor product aerosols produced no statistically significant changes in these enzyme levels. However, a slight effect (possibly, remaining from the 3R4F CS exposure) was noticed in the switch group in the ApoE$^{-/-}$ HnB study.

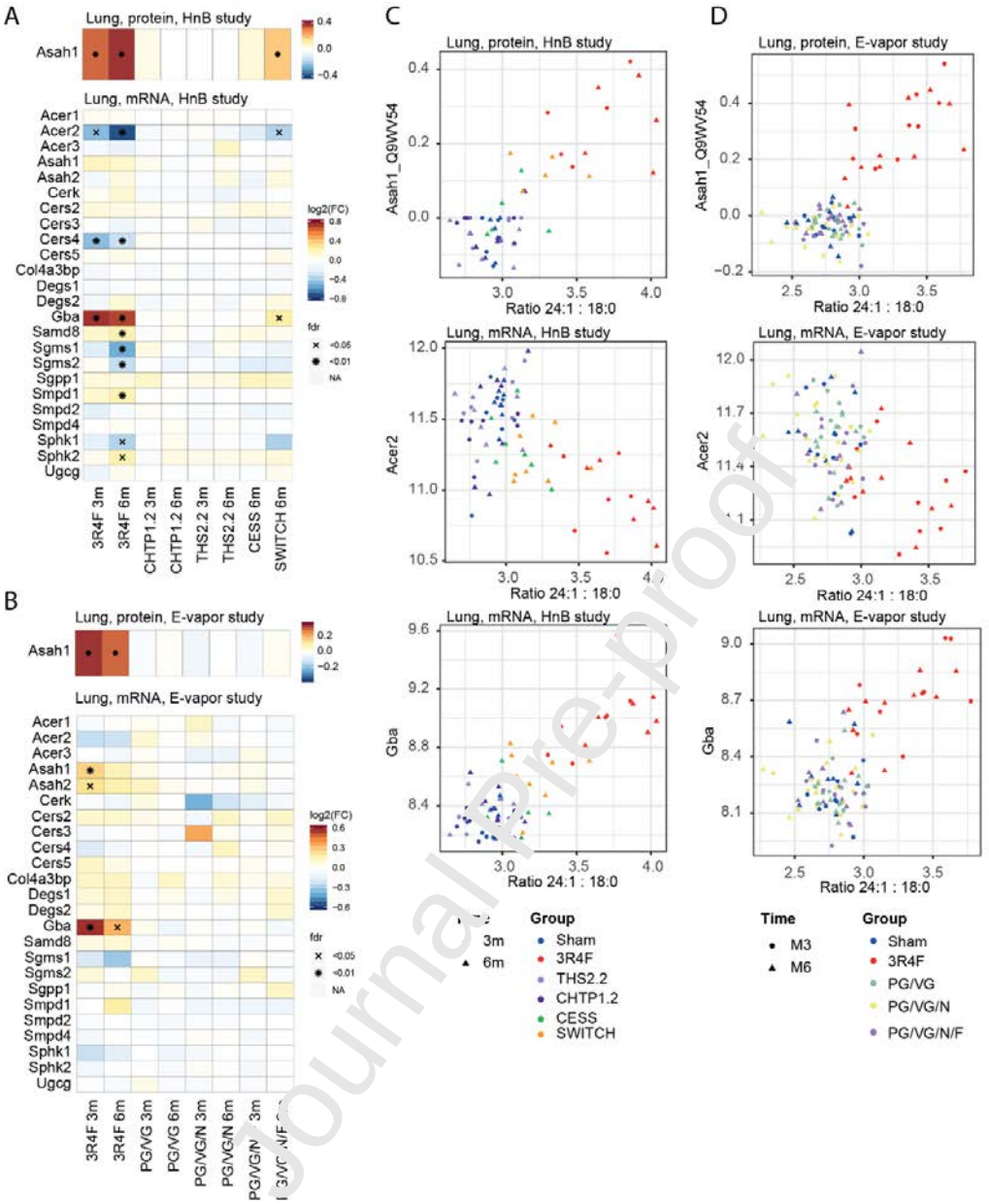

Figure 5. Association between ceramide 24:1/18:0 ratio and protein/gene expression changes. (a) Changes in gene and protein expression of enzymes involved in ceramide metabolism in the ApoE$^{-/-}$ HnB study. Log2 fold changes are color-coded (see key), and statistical significance versus sham exposure is indicated (FDR-adjusted p values: ^{x}<0.05 and *<0.01). Only proteins/genes with significant changes in any of the groups are shown. (b) As in A, but for the ApoE$^{-/-}$ e-vapor study. (c) Scatter plots comparing the measured ceramide 24:1/18:0 ratio with Asah1 protein, Acer2 mRNA, and Gba mRNA expression in the lungs in the ApoE$^{-/-}$ HnB study. The experimental group of each sample is color-coded. (d) As in C, but for the ApoE$^{-/-}$ e-vapor study.

2.5 Consistency in ceramide effects across lipidomics methods and mouse strains

Finally, we analyzed whether the observed effects of CS on ceramide ratios and enzyme levels could be reproduced with a different lipidomics methodology and in WT C57Bl6 mice (in contrast to being specific to the ApoE$^{-/-}$ mouse strain). For this, we leveraged the data generated in two previous system toxicology studies, the first on the effects of a prototype MRTP (pMRTP) in C57Bl6

WT mice and the second on the effects of THS 2.2 in ApoE$^{-/-}$ mice [13]. Although these studies also analyzed ceramide lipidome profiles by LC–MS/MS, their methodology differed from the present one in terms of the lipid extraction protocol and ceramide quantification setup.

To allow direct comparison, we calculated and statistically assessed the same ceramide fractions and ratios as those in the two studies discussed here (Figure 6A). We consistently found that the 24:1 to 18:0 and 24:0 to 18:0 ceramide ratios were significantly elevated in lung tissues upon CS exposure both in the WT and ApoE$^{-/-}$ mouse studies. Similar to the findings in the previously discussed ApoE$^{-/-}$ studies, both ceramide ratios were also significantly increased in the plasma of WT mice upon CS exposure. While both plasma ceramide ratios also demonstrated an increasing trend in the THS 2.2 group in the ApoE$^{-/-}$ study, this increase did not reach significance.

These consistent changes in ceramide ratios were also accompanied by consistent changes in the levels of the core enzymes discussed in the present study: in both studies, Asah1 protein and *Gba* mRNA levels were significantly increased in lung tissues upon CS exposure, whereas *Acer2* mRNA and CerS4 protein levels showed a consistent decrease (Figure 6B).

Overall, the results of re-evaluation of these previously generated ceramide and enzyme profiles further supported the robustness of the ceramide ratio and (select) enzyme responses across different studies, mouse strains, tissues, and lipidomics methods.

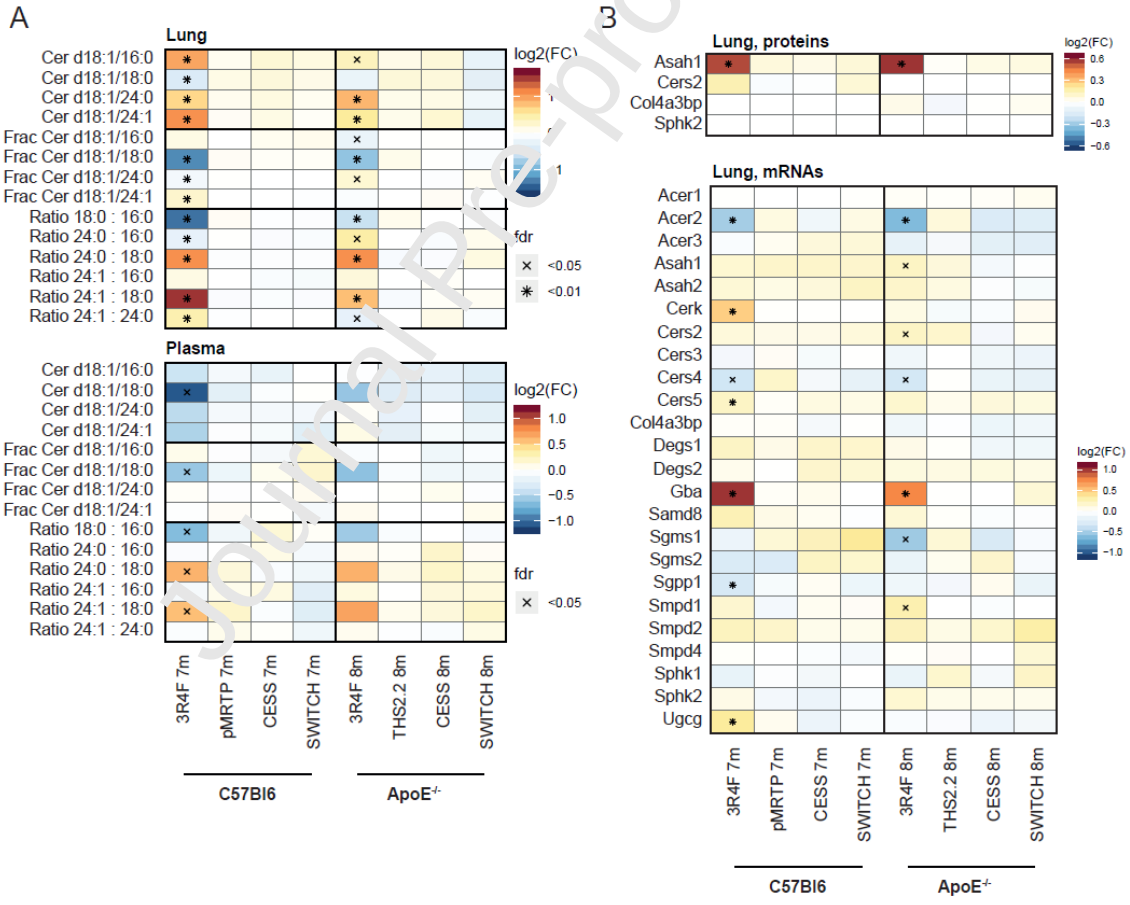

Figure 6. Effects of CS and candidate MRTP aerosols on ceramides and ceramide-related enzymes in previously reported studies on WT C57Bl6 and ApoE$^{-/-}$ mice using different lipidomics methods. Measurements from previous systems toxicology studies on lung and plasma samples [13]. (a) Abundance profiles of different ceramides, relative proportions of ceramides, and some ratios between different species. Fold changes relative to the respective sham group are color-coded, and statistical significance is marked (FDR-adjusted p values: ^{x}<0.05 and *<0.01). Missing values are marked in grey. (b) Changes in gene and protein expression of enzymes involved in ceramide metabolism in these mouse studies.

Discussion

In the current study, we assessed how CS and HnB or e-vapor products aerosols affect the levels of four ceramides in different tissues in mice. Several studies have published evidence on the evaluated ceramides (Cer(d18:1/16:0), Cer(d18:1/18:0), Cer(d18:1/24:0), and Cer(d18:1/24:1(15Z))), particularly, on their clinical relevance in plasma as risk factors of cardiovascular diseases [51, 52], as well as the previously noted chain-length-dependent effect of CS on ceramide levels in mouse lungs [13]. To ensure robust quantification of the selected ceramides, we established and validated an LC–MS/MS-based absolute quantification method, which uses deuterated IS and external calibration curves. We found that CS exposure for 3 months resulted in significantly and substantially elevated ratios of Cer(d18:1/24:0) and Cer(d18:1/24:1) to Cer(d18:1/18:0) in mouse lungs; these results were robustly translatable across four independent studies, including those in ApoE$^{-/-}$ and WT mice (Table 4). The elevation in these ceramide ratios was not limited to the lungs, but also observed in plasma/serum, the liver, and—in case of the Cer(d18:1/24:1) to Cer(d18:1/18:0) ratio—in the abdominal aorta. Concomitant with these ceramide changes, the levels of Asah1 and Gba, which are lysosomal enzymes involved in hydrolysis of glucosylceramides, were consistently elevated in the lungs upon CS exposure. In contrast, neither the tested aerosols from HnB products nor e-vapor product aerosols induced significant changes in the levels of these ceramides or functionally associated enzymes.

Journal Pre-proof

Journal Pre-proof

Table 4. Study overview. The main significantly affected ceramide ratios in the lungs and plasma are shown.

		ApoE$^{-/-}$ HnB study (current)	**ApoE$^{-/-}$ e-vapor study (current)**	**C57Bl6 pMRTP study (previous)**	**ApoE$^{-/-}$ THS study (previous)**
	Mouse strain	ApoE$^{-/-}$	ApoE$^{-/-}$	WT	ApoE$^{-/-}$
	Exposure groups	Sham 3R4F (CS) THS 2.2 CHTP 1.2 Cessation Switch (to CHTP 1.2)	Sham 3R4F (CS) PG/VG PG/VG/N PG/VG/N/F	Sham 3R4F (CS) pMRTP Cessation Switch	Sham 3R4F (CS) THS 2.2 Cessation Switch
	Exposure regimen	Whole body, 3 h per day, 5 days per week	Whole body, 3 h per day, 5 days per week	Whole body, 4 h per day, 5 days per week	Whole body, 3 h per day, 5 days per week
	Matched nicotine exposure dose[1]	28 µg nicotine/L	~35 µg nicotine/L	34.4 µg nicotine/L	29.9 µg nicotine/L
	Total exposure length	6 months	6 months	7 months	8 months
Disease-related endpoints	**Lung inflammation[2]**	↑ (3R4F) → (THS 2.2) → (CHTP 1.2)	↑ (3R4F) → (PG/VG) → (PG/VG/N) → (PG/VG/N/F)	↑ (3R4F) → (pMRTP)	↑ (3R4F) → (THS 2.2)
	Lung emphysema	↑ (3R4F) → (THS 2.2) → (CHTP 1.2)	↑ (3R4F) → (PG/VG) → (PG/VG/N)	↑ (3R4F) → (pMRTP)	↑ (3R4F) → (THS 2.2)

Journal Pre-proof

			→ (PG/VG/N/F)					
	Atherosclerotic plaque formation	↑ (3R4F) → (THS 2.2) → (CHTP 1.2)		↑ (3R4F) → (PG/VG) → (PG/VG/N) → (PG/VG/N/F)		N/A		↑ (3R4F) → (THS 2.2)	
Ceramide ratios	**Tissue**	**Lung**	**Plasma**	**Lung**	**Plasma**	**Lung**	**Plasma**	**Lung**	**Plasma**
	18:0/16:0	↓ (3R4F) → (THS 2.2) → (CHTP 1.2)	→ (3R4F) → (THS 2.2) → (CHTP 1.2)	↓ (3R4F) → (PG/VG) → (PG/VG/N) → (PG/VG/N/F)	→ (3R4F) → (PG/VG) → (PG/VG/N) → (PG/VG/N/F)	↓ (3R4F) → (pMRTP)	↓ (3R4F) → (pMRTP)	↓ (3R4F) → (THS 2.2)	→ (3R4F) → (THS 2.2)
	24:0/18:0	↑ (3R4F) → (THS 2.2) → (CHTP 1.2)	↑ (3R4F) → (THS 2.2) → (CHTP 1.2)	↑ (3R4F) → (PG/VG) → (PG/VG/N) → (PG/VG/N/F)	→ (3R4F) → (PG/VG) → (PG/VG/N) → (PG/VG/N/F)	↑ (3R4F) → (pMRTP)	↑ (3R4F) → (pMRTP)	↑ (3R4F) → (THS 2.2)	→ (3R4F) → (THS 2.2)
	24:1/18:0	↑ (3R4F) → (THS 2.2) → (CHTP 1.2)	↑ (3R4F) → (THS 2.2) → (CHTP 1.2)	↑ (3R4F) → (PG/VG) → (PG/VG/N) → (PG/VG/N/F)	↗ (3R4F) → (PG/VG) → (PG/VG/N) → (PG/VG/N/F)	↑ (3R4F) → (pMRTP)	↑ (3R4F) → (pMRTP)	↑ (3R4F) → (THS 2.2)	→ (3R4F) → (THS 2.2)
	References	**[33]**		**[34]**		**[13, 36]**		**[13, 35]**	

[1]Matched nicotine dose between 3R4F CS and test items, when containing nicotine. [2]As measured by number of inflammatory

Association of ceramides with CS-associated lung diseases. Sphingolipid metabolism plays a key role in the maintenance of normal lung structure and function: Ceramides are the building blocks of functional cellular membranes [61], and sphingolipids are implicated in immunoregulatory functions [62, 63] and in the regulation of diverse physiological processes such as cell turnover, autophagy, and phagocytosis [64, 65].

Ceramides have already been implicated in CS-associated lung diseases. Pulmonary emphysema, induced by CS, importantly contributes to the loss of physiological lung function in COPD. The first evidence of the involvement of ceramides in lung parenchyma damage was presented in the context of apoptosis-dependent emphysema models in mice and rats [26]. In addition, ceramides and sphingosine are produced in increased amounts in alveolar macrophages upon smoking and inhibit the clearance of apoptotic cells by specialized phagocytes [61, 66]. Ceramide accumulation also causes alveolar cell death, for example, via apoptosis [14]. The combination of increased apoptosis and decreased clearance of apoptotic cells is thought to contribute to increased inflammation in the lungs of smokers, by allowing cells to undergo secondary necrosis, resulting in spillage of intracellular contents, chemotaxis of inflammatory cells, and loss of anti-inflammatory phenotypes of alveolar macrophages [67]. The LC–MS/MS profiles of ceramide species in the lungs of mice, rats, and humans indicate that an increase in the absolute levels and a change in the profiles of ceramide species are both associated with emphysema development [26].

Importantly, in all four mouse inhalation studies for which we evaluated the ratios of the four ceramides, we observed substantial lung inflammation and emphysematous changes upon CS exposure (Table 4). In contrast, such disease-related changes were not observed upon HnB or e-vapor products aerosol exposure. On the basis of these ceramide-phenotype associations and the literature referenced above, it is likely that the identified effects of CS on Cer(d18:1/24:0) and Cer(d18:1/24:1) to Cer(d18:1/18:0) ratios in mouse lungs across the four studies reflect the disease-related changes in CS-exposed lung tissues. Of note, while analyses of ceramide levels in COPD patients generally support the relevance of altered ceramide levels in this lung disease, the molecular details—such as the observed ceramide ratios—are not necessarily always fully aligned between human studies and mouse studies. For example, Telenga et al. identified increased levels of 28 ceramides in smokers with COPD versus smokers without COPD in induced sputum samples; however, for example, Cer(d18:1/18:0) and Cer(d18:1/24:0) levels were increased to a similar extent [30]. In plasma, Bowler et al. did identify a negative association between Cer(d18:1/16:0) and emphysema severity in COPD patients, but smoking status was not significantly associated with the measured ceramide levels (Cer(d18:1/16:0), Cer(d18:1/18:0), Cer(d18:1/24:0)) [68]. Overall, despite species/model-specific differences, the shared relevance of ceramides in lung diseases can motivate further mechanistic follow-up studies in mice, for example, to gain further insights into the functional role of altered ceramide ratios.

Relevance of ceramide ratios. Despite the clear overall importance of ceramides, the function of ceramides with different conjugated fatty acids is not clearly defined yet. In the current work, we report significant changes in the ratios of ceramides with different fatty acids in various organ systems upon CS exposure. High levels of ceramides have been reported in people with obesity and type II diabetes [69], and, more specifically, BMI has been reported to be positively associated with Cer(d18:0/18:0) as well as with its ration to Cer(d18:0/24:0), and ceramide cardiovascular risk score [70]. Elevated levels of very-long-chain C24:1 ceramide are associated with aging [71]. Very-long-chain ceramides are, in particular, associated with mitochondrial damage and cell death [72] as well as increase in the serum levels of very-long-chain ceramides was associated with heart failure patients [72, 73]. A number of ceramide species have also been found to be elevated in plasma samples from people with neurodegenerative diseases such as Parkinson disease, Alzheimer disease, dementia, and multiple sclerosis, demonstrating a common signature of Cer(18:1/16:0), Cer (18:1/20:0), and Cer(18:1/24:1(15Z)) [74]. CerS1-deficient mice have decreased levels of d18:1 ceramides with a C18 acyl chain and increased levels of species with other acyl chains (i.e., C16, C20, C22, and C24) relative to

WT mice, and these changes are accompanied by neuronal apoptosis in the cerebellum [75]. Finally, experiments with CerS2 knockout mice have revealed the crucial role of ceramide balance in maintaining lung homeostasis, demonstrating a phenotype of accumulation of foamy alveolar macrophages and increased lung volume, possibly caused by a strong compensatory accumulation of Cer(d18:1/16:0) [76].

Thus, on the basis of this evidence for the imbalance of ceramides under various disease conditions, ceramide ratios may be considered as potential prognostic markers. In fact, ceramides have been implemented as clinical biomarkers for large-scale screening for cardiovascular diseases [13]. The Mayo Clinic verified that ceramide ratios measured in a clinical assay are predictive of the risk of cardiovascular disease [77]. The concentrations of Cer(d18:1/16:0), Cer(d18:1/18:0), Cer(d18:1/24:0), and Cer(d18:1/24:1(15Z)) and, in particular, the ratio of Cer(d18:1/16:0)/Cer(d18:1/24:0) are associated with a higher risk of cardiovascular death in patients with stable coronary artery disease and acute coronary syndromes beyond low-density lipoprotein-cholesterol [13].

Possible mechanistic contributions to the observed effects on ceramide ratios. The observed ceramide changes upon CS exposure were only partially explainable by the changes in relevant enzyme levels (see Supplementary Text). The observed upregulation of Gba and Asah1 and downregulation of Cers4 and Acer2 in the lungs suggest that CS distorts the molecular profile of the different ceramides in multiple ways, resulting, overall, in the observed changes in ceramide ratios. In addition, the upregulation of acidic lysosomal enzymes (such as Gba and Asah1) upon CS exposure supports the possibility of increased ceramide turnover through the salvage pathway in the lysosomes.

With the lungs as the first and primary target of CS-induced biological effects, it is likely that ceramide changes induced in the lungs can directly spillover to plasma/serum. Similarly, ceramide exchange between the lungs and liver might explain the observed effects of CS exposure on ceramide levels in the liver. However, other explanations are possible, including the (more direct) effects of CS exposure on ceramide metabolic pathways in the liver, for example, including the observed downregulation of Cerk, which converts ceramides to ceramide phosphate.

Study limitations. The strengths of the current study include the use of a robust and validated lipidomics assay and reproducible identification of changes in ceramide ratios in four independent studies, both in ApoE$^{-/-}$ and WT mice. While ceramide changes were associated with disease-related changes in these mouse studies (Table 4; e.g., lung emphysema), a core question that we did not address directly in the current study is whether and to what extent similar changes in ceramide ratios also occur in human smokers and/or smoking-induced diseases. Thus, the current work does not directly inform about the human situation. However, as discussed above, at least an association between ceramide levels and COPD appears possible [30, 68]. Additionally, our study did not distill a clear mechanism how CS exposure results in a significant increase in ratios of Cer(d18:1/24:0) and Cer(d18:1/24:1(15Z)) versus Cer(d18:1/18:0), although our discussion lays out possible mechanisms. A better understanding of the causality chain in this mouse model could help guide mechanistic explanations for the observations in clinical studies. However, this will require more detailed follow-up experiments in separate studies—possibly including cell-type-resolved ceramide and enzyme measurements (e.g., [78]), isotope-labeling approaches to trace the origin of the changes (e.g. [79, 80]), and measurement of the full sphingolipid pathway pool (including sphingosine, sphingosine phosphate, ceramide phosphate, galactosyl/glucosyl, sphingomyelin, dehydroceramides, and globosides)—in a fully validated manner, supported by further mechanistic investigations in complementary *in vitro* model systems. In addition, expansion of the current ceramide panel to other sphingolipids would be relevant, as indicated by previous results from mouse [13] and human studies [81].

5. Conclusions

In the current work, we established, validated and automatized a ceramide *quantification* assay suitable for large scale toxicological and clinical studies. *Across four independent mouse studies* we identified the ratios of Cer(d18:1/24:0) and Cer(d18:1/24:1(15Z)) to Cer(d18:1/18:0) as markers of CS exposure in the lungs, plasma, and liver. *Concurrently*, we observed no statistically significant effect following exposure to aerosols generated by two heat-not-burn tobacco products or to e-vapor aerosols *as well as* the full recovery of perturbed ceramide profiles after 3 months of smoking cessation. Similarly, the CS-induced effects on ceramide profiles reverted toward sham levels upon switching to potential MRTPs. With this, our results for *mice* contributes to the accumulating evidence supporting the relevance of ceramide ratios as markers of biological effects [19, 82]. *However, the long-term metabolic changes and health risks for humans associated with the usage of modified risk tobacco products have not been assessed in these mouse studies*.

Supplementary Materials: Supplementary materials can be found at www.mdpi.com/xxx/s1

Author Contributions: Conceptualization, O.L., J.H., N.I. and B.T.; methodology, O.L., K.E.; software, B.T., A.K.; validation, D.S., O.L., S.D., A.K; formal analysis, B.T., A.K.; investigation, O.L., S.D., C.N., E.G.; resources, B.P.; writing—original draft preparation, B.T., O.L.; writing—review and editing, all; visualization, B.T., A.K; supervision, O.L, T.S., E.G., B.P., F.M., M.P., J.H., N.I.; project administration, B.T., J.S., B.P. All authors have read and agreed to the published version of the manuscript.

Acknowledgments: The authors would like to thank the study team and especially acknowledge the technical assistance and support of the bioresearch and aerosol teams at PMI R&D, Philip Morris International Research Laboratories Pte. Ltd., Singapore, and PMI R&D, Philip Morris Products S.A., Neuchâtel, Switzerland. The authors thank Sam Ansari for managing the biobanking and acknowledge the support of Sindhoora Bhargavi Gopala Reddy for editing a draft of the manuscript.

Conflicts of Interest: The work reported in this publication involved candidate/potential modified risk tobacco products developed by Philip Morris International. Philip Morris International is the sole source of funding and sponsor of this research. Except K.E., all authors are employees of PMI R&D or had worked for PMI R&D under contractual agreements. K.E. is an employee of Lipidomics Consulting Ltd.

Abbreviations

MRTP	Modified risk tobacco product
CS	Cigarette smoke
HnB	Heat not burn
ECIG	Electronic cigarette
CHTP	Carbon Heating Tobacco System
THS	Tobacco Heating System
VG	Vegetable glycerin
PG	Propylene glycol
N	Nicotine
F	Flavor
QC	Quality control
Cer	Ceramide
COPD	Chronic obstructive pulmonary disease

References

1. Martin, P.; Glasgow, H.; Patterson, J., Chronic obstructive pulmonary disease (COPD): smoking remains the most important cause. *N Z Med J* **2005,** 118, (1213), U1409.
2. Lubin, J. H.; Couper, D.; Lutsey, P. L.; Woodward, M.; Yatsuya, H.; Huxley, R. R., Risk of Cardiovascular Disease from Cumulative Cigarette Use and the Impact of Smoking Intensity. *Epidemiology* **2016,** 27, (3), 395-404.

3. Godtfredsen, N.; Lam, T.; Hansel, T.; Leon, M.; Gray, N.; Dresler, C.; Burns, D.; Prescott, E.; Vestbo, J., COPD-related morbidity and mortality after smoking cessation: status of the evidence. *European Respiratory Journal* **2008,** 32, (4), 844-853.
4. Smith, M. R.; Clark, B.; Lüdicke, F.; Schaller, J.-P.; Vanscheeuwijck, P.; Hoeng, J.; Peitsch, M. C., Evaluation of the Tobacco Heating System 2.2. Part 1: Description of the system and the scientific assessment program. *Regulatory Toxicology and Pharmacology* **2016,** 81, S17-S26.
5. Titz, B.; Kogel, U.; Martin, F.; Schlage, W. K.; Xiang, Y.; Nury, C.; Dijon, S.; Baumer, K.; Peric, D.; Bornand, D.; Dulize, R.; Phillips, B.; Leroy, P.; Vuillaume, G.; Lebrun, S.; Elamin, A.; Guedj, E.; Trivedi, K.; Ivanov, N. V.; Vanscheeuwijck, P.; Peitsch, M. C.; Hoeng, J., A 90-day OECD TG 413 rat inhalation study with systems toxicology endpoints demonstrates reduced exposure effects of the aerosol from the carbon heated tobacco product version 1.2 (CHTP1.2) compared with cigarette smoke. II. Systems toxicology assessment. *Food Chem Toxicol* **2018,** 115, 284-301.
6. Tayyarah, R.; Long, G. A., Comparison of select analytes in aerosol from e-cigarettes with smoke from conventional cigarettes and with ambient air. *Regul Toxicol Pharmacol* **2014,** 70, (3), 704-10.
7. Goniewicz, M. L.; Knysak, J.; Gawron, M.; Kosmider, L.; Sobczak, A.; Kurek, J.; Prokopowicz, A.; Jablonska-Czapla, M.; Rosik-Dulewska, C.; Havel, C.; Jacob, P., 3rd; Benowitz, N., Levels of selected carcinogens and toxicants in vapour from electronic cigarettes. *Tob Control* **2014,** 23, (2), 133-9.
8. Marco, E.; Grimalt, J. O., A rapid method for the chromatographic analysis of volatile organic compounds in exhaled breath of tobacco cigarette and electronic cigarette smokers. *J Chromatogr A* **2015,** 1410, 51-9.
9. Hecht, S. S.; Carmella, S. G.; Kotandeniya, D.; Pillsbury, M. E.; Chen, M.; Ransom, B. W.; Vogel, R. I.; Thompson, E.; Murphy, S. E.; Hatsukami, D. K., Evaluation of toxicant and carcinogen metabolites in the urine of e-cigarette users versus cigarette smokers. *Nicotine Tob Res* **2015,** 17, (6), 704-9.
10. Schaller, J.-P.; Keller, D.; Poget, L.; Pratte, P.; Kaelin, E.; McHugh, D.; Cudazzo, G.; Smart, D.; Tricker, A. R.; Gautier, L., Evaluation of the Tobacco Heating System 2.2. Part 2: Chemical composition, genotoxicity, cytotoxicity, and physical properties of the aerosol. *Regulatory Toxicology and Pharmacology* **2016,** 81, S27-S47.
11. Phillips, B. W.; Schlage, W. K.; Titz, B.; Kogel, U.; Sciuscio, D.; Martin, F.; Leroy, P.; Vuillaume, G.; Krishnan, S.; Lee, T.; Veljkovic, E.; Elamin, A.; Merg, C.; Ivanov, N. V.; Peitsch, M. C.; Hoeng, J.; Vanscheeuwijck, P., A 90-day OECD TG 413 rat inhalation study with systems toxicology endpoints demonstrates reduced exposure effects of the aerosol from the carbon heated tobacco product version 1.2 (CHTP1.2) compared with cigarette smoke. I. Inhalation exposure, clinical pathology and histopathology. *Food and chemical toxicology : an international journal published for the British Industrial Biological Research Association* **2018,** 115, (Pt B), 388-413.
12. Lee, G.; Walser, T. C.; Dubinett, S. M., Chronic inflammation, chronic obstructive pulmonary disease, and lung cancer. *Curr Opin Pulm Med* **2009,** 15, (4), 303-7.
13. Titz, B.; Boue, S.; Phillips, B.; Talikka, M.; Vihervaara, T.; Schneider, T.; Nury, C.; Elamin, A.; Guedj, E.; Peck, M. J.; Schlage, W. K.; Cabanski, M.; Leroy, P.; Vuillaume, G.; Martin, F.; Ivanov, N. V.; Veljkovic, E.; Ekroos, K.; Laaksonen, R.; Vanscheeuwijck, P.; Peitsch, M. C.; Hoeng, J., Effects of Cigarette Smoke, Cessation, and Switching to Two Heat-Not-Burn Tobacco Products on Lung Lipid Metabolism in C57BL/6 and Apoe-/- Mice-An Integrative Systems Toxicology Analysis. *Toxicological sciences* **2016,** 149, (2), 441-57.
14. Ghidoni, R.; Caretti, A.; Signorelli, P., Role of Sphingolipids in the Pathobiology of Lung Inflammation. *Mediators Inflamm* **2015,** 2015, 487508.
15. Park, K.; Elias, P. M.; Shin, K. O.; Lee, Y. M.; Hupe, M.; Borkowski, A. W.; Gallo, R. L.; Saba, J.; Holleran, W. M.; Uchida, Y., A novel role of a lipid species, sphingosine-1-phosphate, in epithelial innate immunity. *Molecular and cellular biology* **2013,** 33, (4), 752-62.
16. Mundra, P. A.; Barlow, C. K.; Nestel, P. J.; Barnes, E. H.; Kirby, A.; Thompson, P.; Sullivan, D. R.; Alshehry, Z. H.; Mellett, N. A.; Huynh, K.; Jayawardana, K. S.; Giles, C.; McConville, M. J.; Zoungas, S.; Hillis, G. S.; Chalmers, J.; Woodward, M.; Wong, G.; Kingwell, B. A.; Simes, J.; Tonkin, A. M.; Meikle, P. J.; Investigators, L. S., Large-scale plasma lipidomic profiling identifies lipids that predict cardiovascular events in secondary prevention. *JCI Insight* **2018,** 3, (17).
17. Laaksonen, R.; Ekroos, K.; Sysi-Aho, M.; Hilvo, M.; Vihervaara, T.; Kauhanen, D.; Suoniemi, M.; Hurme, R.; Marz, W.; Scharnagl, H.; Stojakovic, T.; Vlachopoulou, E.; Lokki, M. L.; Nieminen, M. S.; Klingenberg, R.; Matter, C. M.; Hornemann, T.; Juni, P.; Rodondi, N.; Raber, L.; Windecker, S.; Gencer, B.; Pedersen, E. R.; Tell, G. S.; Nygard, O.; Mach, F.; Sinisalo, J.; Luscher, T. F., Plasma ceramides predict cardiovascular

death in patients with stable coronary artery disease and acute coronary syndromes beyond LDL-cholesterol. *European heart journal* **2016,** 37, (25), 1967-76.

18. Mantovani, A.; Bonapace, S.; Lunardi, G.; Canali, G.; Dugo, C.; Vinco, G.; Calabria, S.; Barbieri, E.; Laaksonen, R.; Bonnet, F.; Byrne, C. D.; Targher, G., Associations between specific plasma ceramides and severity of coronary-artery stenosis assessed by coronary angiography. *Diabetes & Metabolism* **2019**.
19. Poss, A. M.; Maschek, J. A.; Cox, J. E.; Hauner, B. J.; Hopkins, P. N.; Hunt, S. C.; Holland, W. L.; Summers, S. A.; Playdon, M. C., Machine Learning Reveals Serum Sphingolipids as Cholesterol-Independent Biomarkers of Coronary Artery Disease. *The Journal of Clinical Investigation* **2019**.
20. Perrotti, F.; Rosa, C.; Cicalini, I.; Sacchetta, P.; Del Boccio, P.; Genovesi, D.; Pieragostino, D., Advances in Lipidomics for Cancer Biomarkers Discovery. *International journal of molecular sciences* **2016,** 17, (12).
21. Dodge, J. C., Lipid Involvement in Neurodegenerative Diseases of the Motor System: Insights from Lysosomal Storage Diseases. *Front Mol Neurosci* **2017,** 10, 356.
22. Galadari, S.; Rahman, A.; Pallichankandy, S.; Galadari, A.; Thayyullathil, F., Role of ceramide in diabetes mellitus: evidence and mechanisms. *Lipids Health Dis* **2013,** 12, 98.
23. Grassme, H.; Becker, K. A., Bacterial infections and ceramide. *Handb Exp Pharmacol* **2013**, (216), 305-20.
24. Gomez-Munoz, A.; Presa, N.; Gomez-Larrauri, A.; Rivera, I. G.; Trueba, M.; Ordonez, M., Control of inflammatory responses by ceramide, sphingosine 1-phosphate and ceramide 1-phosphate. *Prog Lipid Res* **2016,** 61, 51-62.
25. Schweitzer, K. S.; Hatoum, H.; Brown, M. B.; Gupta, M.; Justice, M. J.; Beteck, B.; Van Demark, M.; Gu, Y.; Presson, R. G., Jr.; Hubbard, W. C.; Petrache, I., Mechanisms of lung endothelial barrier disruption induced by cigarette smoke: role of oxidative stress and ceramides. *Am J Physiol Lung Cell Mol Physiol* **2011,** 301, (6), L836-46.
26. Petrache, I.; Natarajan, V.; Zhen, L.; Medler, T. R.; Richter, A. T.; Cho, C.; Hubbard, W. C.; Berdyshev, E. V.; Tuder, R. M., Ceramide upregulation causes pulmonary cell apoptosis and emphysema-like disease in mice. *Nature medicine* **2005,** 11, (5), 491-8.
27. Pilecki, B.; Wulf-Johansson, H.; Støttrup, C.; Jørgensen, P. T.; Djiadeu, P.; Nexøe, A. B.; Schlosser, A.; Hansen, S. W. K.; Madsen, J.; Clark, H. W., Surfactant protein D deficiency aggravates cigarette smoke-induced lung inflammation by upregulation of ceramide synthesis. *Frontiers in immunology* **2018,** 9, 3013.
28. Zulueta, A.; Caretti, A.; Campisi, G. M.; Bizzolari, A.; Abad, J. L.; Paroni, R.; Signorelli, P.; Ghidoni, R., Inhibitors of ceramide de novo biosynthesis rescue damages induced by cigarette smoke in airways epithelia. *Naunyn-Schmiedeberg's archives of pharmacology* **2017,** 390, (7), 753-759.
29. Tippetts, T. S.; Winden, D. R.; Swensen, A. C.; Nelson, M. B.; Thatcher, M. O.; Saito, R. R.; Condie, T. B.; Simmons, K. J.; Judd, A. M.; Reynolds, P. R., Cigarette smoke increases cardiomyocyte ceramide accumulation and inhibits mitochondrial respiration. *BMC cardiovascular disorders* **2014,** 14, (1), 165.
30. Telenga, E. D.; Hoffmann, R. F.; Ruben, t. K.; Hoonhorst, S. J.; Willemse, B. W.; van Oosterhout, A. J.; Heijink, I. H.; van den Berge, M.; Jorge, L.; Sandra, P.; Postma, D. S.; Sandra, K.; ten Hacken, N. H., Untargeted lipidomic analysis in chronic obstructive pulmonary disease. Uncovering sphingolipids. *Am J Respir Crit Care Med* **2014,** 190, (2), 155-64.
31. Meir, K. S.; Leitersdorf, E., Atherosclerosis in the apolipoprotein-E-deficient mouse: a decade of progress. *Arteriosclerosis, thrombosis, and vascular biology* **2004,** 24, (6), 1006-14.
32. Boue, S.; De Leon, H.; Schlage, W. K.; Peck, M. J.; Weiler, H.; Berges, A.; Vuillaume, G.; Martin, F.; Friedrichs, B.; Lebrun, S.; Meurrens, K.; Schracke, N.; Moehring, M.; Steffen, Y.; Schueller, J.; Vanscheeuwijck, P.; Peitsch, M. C.; Hoeng, J., Cigarette smoke induces molecular responses in respiratory tissues of ApoE(-/-) mice that are progressively deactivated upon cessation. *Toxicology* **2013,** 314, (1), 112-24.
33. Phillips, B.; Szostak, J.; Titz, B.; Schlage, W. K.; Guedj, E.; Leroy, P.; Vuillaume, G.; Martin, F.; Buettner, A.; Elamin, A.; Sewer, A.; Sierro, N.; Choukrallah, M. A.; Schneider, T.; Ivanov, N. V.; Teng, C.; Tung, C. K.; Lim, W. T.; Yeo, Y. S.; Vanscheeuwijck, P.; Peitsch, M. C.; Hoeng, J., A six-month systems toxicology inhalation/cessation study in ApoE(-/-) mice to investigate cardiovascular and respiratory exposure effects of modified risk tobacco products, CHTP 1.2 and THS 2.2, compared with conventional cigarettes. *Food and chemical toxicology : an international journal published for the British Industrial Biological Research Association* **2019,** 126, 113-141.
34. Szostak, J.; Wong, E. T.; Titz, B.; Lee, T.; Wong, S. K.; Low, T.; Lee, K. M.; Zhang, J.; Kumar, A.; Schlage, W. K.; Guedj, E.; Phillips, B.; Leroy, P.; Buettner, A.; Xiang, Y.; Martin, F.; Sewer, A.; Kuczaj, A.; Ivanov, N. V.; Luettich, K.; Vanscheeuwijck, P.; Peitsch, M. C.; Hoeng, J., A 6-month systems toxicology inhalation study in ApoE-/- mice demonstrates reduced cardiovascular effects of E-vapor aerosols compared to cigarette smoke. *American journal of physiology. Heart and circulatory physiology* **2020**.

35. Phillips, B.; Veljkovic, E.; Boue, S.; Schlage, W. K.; Vuillaume, G.; Martin, F.; Titz, B.; Leroy, P.; Buettner, A.; Elamin, A.; Oviedo, A.; Cabanski, M.; De Leon, H.; Guedj, E.; Schneider, T.; Talikka, M.; Ivanov, N. V.; Vanscheeuwijck, P.; Peitsch, M. C.; Hoeng, J., An 8-Month Systems Toxicology Inhalation/Cessation Study in Apoe-/- Mice to Investigate Cardiovascular and Respiratory Exposure Effects of a Candidate Modified Risk Tobacco Product, THS 2.2, Compared With Conventional Cigarettes. *Toxicological sciences : an official journal of the Society of Toxicology* **2016,** 151, (2), 462-4.
36. Phillips, B.; Veljkovic, E.; Peck, M. J.; Buettner, A.; Elamin, A.; Guedj, E.; Vuillaume, G.; Ivanov, N. V.; Martin, F.; Boue, S.; Schlage, W. K.; Schneider, T.; Titz, B.; Talikka, M.; Vanscheeuwijck, P.; Hoeng, J.; Peitsch, M. C., A 7-month cigarette smoke inhalation study in C57BL/6 mice demonstrates reduced lung inflammation and emphysema following smoking cessation or aerosol exposure from a prototypic modified risk tobacco product. *Food and chemical toxicology : an international journal published for the British Industrial Biological Research Association* **2015,** 80, 328-345.
37. Lofgren, L.; Forsberg, G. B.; Stahlman, M., The BUME method: a new rapid and simple chloroform-free method for total lipid extraction of animal tissue. *Scientific reports* **2016,** 6, 27688.
38. Lofgren, L.; Stahlman, M.; Forsberg, G. B.; Saarinen, S.; Nilsson, R.; Hansson, G. I., The BUME method: a novel automated chloroform-free 96-well total lipid extraction method for blood plasma. *Journal of lipid research* **2012,** 53, (8), 1690-700.
39. Qu, F.; Zhang, H.; Zhang, M.; Hu, P., Sphingolipidomic Profiling of Rat Serum by UPLC-Q-TOF-MS: Application to Rheumatoid Arthritis Study. *Molecules* **2018,** 23, (3).
40. Burla, B.; Arita, M.; Arita, M.; Bendt, A. K.; Cazenave-Gassiot, A.; Dennis, E. A.; Ekroos, K.; Han, X.; Ikeda, K.; Liebisch, G.; Lin, M. K.; Loh, T. P.; Meikle, P. J.; Oresic, M.; Quehenberger, O.; Shevchenko, A.; Torta, F.; Wakelam, M. J. O.; Wheelock, C. E.; Wenk, M. R., MS-based lipidomics of human blood plasma: a community-initiated position paper to develop accepted guidelines. *Journal of lipid research* **2018,** 59, (10), 2001-2017.
41. Ribbenstedt, A.; Ziarrusta, H.; Benskin, J. P., Development, characterization and comparisons of targeted and non-targeted metabolomics methods. *PloS one* **2018,** 13, (11), e0207082.
42. Bligh, E. G.; Dyer, W. J., A rapid method of total lipid extraction and purification. *Canadian journal of biochemistry and physiology* **1959,** 37, (8), 911-7.
43. Matyash, V.; Liebisch, G.; Kurzchalia, T. V.; Shevchenko, A.; Schwudke, D., Lipid extraction by methyl-tert-butyl ether for high-throughput lipidomics. *Journal of lipid research* **2008,** 49, (5), 1137-46.
44. Mee, R. W., β-expectation and β-content tolerance limits for balanced one-way ANOVA random model. *Technometrics* **1984,** 26, (3), 251-254.
45. R Development Core Team *R: A Language and Environment for Statistical Computing*, 2007.
46. Gentleman, R. C.; Carey, V. J.; Bates, D. M.; Bolstad, B.; Dettling, M.; Dudoit, S.; Ellis, B.; Gautier, L.; Ge, Y.; Gentry, J.; Hornik, K.; Hothorn, T.; Huber, W.; Iacus, S.; Irizarry, R.; Leisch, F.; Li, C.; Maechler, M.; Rossini, A. J.; Sawitzki, G.; Smith, C.; Smyth, G.; Tierney, L.; Yang, J. Y.; Zhang, J., Bioconductor: open software development for computational biology and bioinformatics. *Genome Biol* **2004,** 5, (10), R80.
47. Kelstrup, C. D.; Jersie-Christensen, R. R.; Batth, T. S.; Arrey, T. N.; Kuehn, A.; Kellmann, M.; Olsen, J. V., Rapid and deep proteomes by faster sequencing on a benchtop quadrupole ultra-high-field Orbitrap mass spectrometer. *Journal of proteome research* **2014,** 13, (12), 6187-6195.
48. Huber, W.; Von Heydebreck, A.; Sültmann, H.; Poustka, A.; Vingron, M., Variance stabilization applied to microarray data calibration and to the quantification of differential expression. *Bioinformatics* **2002,** 18, (suppl 1), S96-S104.
49. Hultin-Rosenberg, L.; Forshed, J.; Branca, R. M.; Lehtio, J.; Johansson, H. J., Defining, comparing, and improving iTRAQ quantification in mass spectrometry proteomics data. *Molecular & cellular proteomics : MCP* **2013,** 12, (7), 2021-31.
50. Herbrich, S. M.; Cole, R. N.; West Jr, K. P.; Schulze, K.; Yager, J. D.; Groopman, J. D.; Christian, P.; Wu, L.; O'Meally, R. N.; May, D. H.; McIntosh, M.; Ruczinski, I., Statistical Inference from Multiple iTRAQ Experiments without Using Common Reference Standards. *Journal of proteome research* **2013,** 12, (2), 594-604.
51. Havulinna, A. S.; Sysi-Aho, M.; Hilvo, M.; Kauhanen, D.; Hurme, R.; Ekroos, K.; Salomaa, V.; Laaksonen, R., Circulating Ceramides Predict Cardiovascular Outcomes in the Population-Based FINRISK 2002 Cohort. *Arteriosclerosis, thrombosis, and vascular biology* **2016,** 36, (12), 2424-2430.
52. Meikle, P. J.; Formosa, M. F.; Mellett, N. A.; Jayawardana, K. S.; Giles, C.; Bertovic, D. A.; Jennings, G. L.; Childs, W.; Reddy, M.; Carey, A. L.; Baradi, A.; Nanayakkara, S.; Wilson, A. M.; Duffy, S. J.; Kingwell, B. A., HDL Phospholipids, but Not Cholesterol Distinguish Acute Coronary Syndrome From Stable Coronary Artery Disease. *J Am Heart Assoc* **2019,** 8, (11), e011792.

53. Guideline, I. H. T. In *Validation of analytical procedures: text and methodology Q2 (R1)*, International conference on harmonization, Geneva, Switzerland, 2005; 2005; pp 11-12.
54. FDA Bioanalytical Method Validation, Guidance for Industry. https://www.fda.gov/regulatory-information/search-fda-guidance-documents/bioanalytical-method-validation-guidance-industry
55. Kauhanen, D.; Sysi-Aho, M.; Koistinen, K. M.; Laaksonen, R.; Sinisalo, J.; Ekroos, K., Development and validation of a high-throughput LC-MS/MS assay for routine measurement of molecular ceramides. *Analytical and bioanalytical chemistry* **2016,** 408, (13), 3475-83.
56. Baudoin-Dehoux, C.; Castellan, T.; Rodriguez, F.; Rives, A.; Stauffert, F.; Garcia, V.; Levade, T.; Compain, P.; Genisson, Y., Selective Targeting of the Interconversion between Glucosylceramide and Ceramide by Scaffold Tailoring of Iminosugar Inhibitors. *Molecules* **2019,** 24, (2).
57. Coant, N.; Sakamoto, W.; Mao, C.; Hannun, Y. A., Ceramidases, roles in sphingolipid metabolism and in health and disease. *Adv Biol Regul* **2017,** 63, 122-131.
58. Levy, M.; Futerman, A. H., Mammalian ceramide synthases. *IUBMB Life* **2010,** 62, (5), 347-56.
59. Sugiura, M.; Kono, K.; Liu, H.; Shimizugawa, T.; Minekura, H.; Spiegel, S.; Kohama, T., Ceramide kinase, a novel lipid kinase. Molecular cloning and functional characterization. *The Journal of biological chemistry* **2002,** 277, (26), 23294-300.
60. Gault, C. R.; Obeid, L. M.; Hannun, Y. A., An overview of sphingolipid metabolism: from synthesis to breakdown. *Advances in experimental medicine and biology* **2010,** 688, 1-23.
61. Justice, M. J.; Petrusca, D. N.; Rogozea, A. L.; Williams, J. A.; Schweitzer, K. S.; Petrache, I.; Wassall, S. R.; Petrache, H. I., Effects of lipid interactions on model vesicle engulfment by alveolar macrophages. *Biophys J* **2014,** 106, (3), 598-609.
62. Spiegel, S.; Milstien, S., The outs and the ins of sphingosine-1-phosphate in immunity. *Nature reviews. Immunology* **2011,** 11, (6), 403-15.
63. Rosen, H.; Goetzl, E. J., Sphingosine 1-phosphate and its receptors: an autocrine and paracrine network. *Nature reviews. Immunology* **2005,** 5, (7), 560-70.
64. Pinto, S. N.; Laviad, E. L.; Stiban, J.; Kelly, S. L.; Merrill, A. H., Jr.; Prieto, M.; Futerman, A. H.; Silva, L. C., Changes in membrane biophysical properties induced by sphingomyelinase depend on the sphingolipid N-acyl chain. *Journal of lipid research* **2014,** 55, (1), 53-61.
65. Hannun, Y. A.; Obeid, L. M., Principles of bioactive lipid signalling: lessons from sphingolipids. *Nature reviews. Molecular cell biology* **2008,** 9, (2), 139-50.
66. Petrusca, D. N.; Gu, Y.; Adamowicz, J. J.; Rush, N. I.; Hubbard, W. C.; Smith, P. A.; Berdyshev, E. V.; Birukov, K. G.; Lee, C. H.; Tuder, R. M.; Twigg, H. L., 3rd; Vandivier, R. W.; Petrache, I., Sphingolipid-mediated inhibition of apoptotic cell clearance by alveolar macrophages. *The Journal of biological chemistry* **2010,** 285, (51), 40322-32.
67. Korns, D.; Frasch, S. C.; Fernandez-Boyanapalli, R.; Henson, P. M.; Bratton, D. L., Modulation of macrophage efferocytosis in inflammation. *Front Immunol* **2011,** 2, 57.
68. Bowler, R. P.; Jacobson, S.; Cruickshank, C.; Hughes, G. J.; Siska, C.; Ory, D. S.; Petrache, I.; Schaffer, J. E.; Reisdorph, N.; Kechris, K., Plasma sphingolipids associated with chronic obstructive pulmonary disease phenotypes. *Am J Respir Crit Care Med* **2015,** 191, (3), 275-84.
69. Gomez-Munoz, A.; Gangoiti, P.; Granado, M. H.; Arana, L.; Ouro, A., Ceramide-1-phosphate in cell survival and inflammatory signaling. *Advances in experimental medicine and biology* **2010,** 688, 118-30.
70. Drazba, M. A.; Holaskova, I.; Sahyoun, N. R.; Ventura Marra, M., Associations of Adiposity and Diet Quality with Serum Ceramides in Middle-Aged Adults with Cardiovascular Risk Factors. *J Clin Med* **2019,** 8, (4).
71. Khayrullin, A.; Krishnan, P.; Martinez-Nater, L.; Mendhe, B.; Fulzele, S.; Liu, Y.; Mattison, J. A.; Hamrick, M. W., Very Long-Chain C24:1 Ceramide Is Increased in Serum Extracellular Vesicles with Aging and Can Induce Senescence in Bone-Derived Mesenchymal Stem Cells. *Cells* **2019,** 8, (1).
72. Law, B. A.; Liao, X.; Moore, K. S.; Southard, A.; Roddy, P.; Ji, R.; Szulc, Z.; Bielawska, A.; Schulze, P. C.; Cowart, L. A., Lipotoxic very-long-chain ceramides cause mitochondrial dysfunction, oxidative stress, and cell death in cardiomyocytes. *FASEB J* **2018,** 32, (3), 1403-1416.
73. Ji, R.; Akashi, H.; Drosatos, K.; Liao, X.; Jiang, H.; Kennel, P. J.; Brunjes, D. L.; Castillero, E.; Zhang, X.; Deng, L. Y.; Homma, S.; George, I. J.; Takayama, H.; Naka, Y.; Goldberg, I. J.; Schulze, P. C., Increased de novo ceramide synthesis and accumulation in failing myocardium. *JCI Insight* **2017,** 2, (14).
74. Pujol-Lereis, L. M., Alteration of Sphingolipids in Biofluids: Implications for Neurodegenerative Diseases. *International journal of molecular sciences* **2019,** 20, (14).
75. Ginkel, C.; Hartmann, D.; vom Dorp, K.; Zlomuzica, A.; Farwanah, H.; Eckhardt, M.; Sandhoff, R.; Degen, J.; Rabionet, M.; Dere, E.; Dormann, P.; Sandhoff, K.; Willecke, K., Ablation of neuronal ceramide

Journal Pre-proof

synthase 1 in mice decreases ganglioside levels and expression of myelin-associated glycoprotein in oligodendrocytes. *The Journal of biological chemistry* **2012,** 287, (50), 41888-902.

76. Petrache, I.; Kamocki, K.; Poirier, C.; Pewzner-Jung, Y.; Laviad, E. L.; Schweitzer, K. S.; Van Demark, M.; Justice, M. J.; Hubbard, W. C.; Futerman, A. H., Ceramide synthases expression and role of ceramide synthase-2 in the lung: insight from human lung cells and mouse models. *PLoS One* **2013,** 8, (5), e62968.
77. Tippetts, T. S.; Holland, W. L.; Summers, S. A., The ceramide ratio: a predictor of cardiometabolic risk. *Journal of lipid research* **2018,** 59, (9), 1549-1550.
78. Shin, K. C.; Hwang, I.; Choe, S. S.; Park, J.; Ji, Y.; Kim, J. I.; Lee, G. Y.; Choi, S. H.; Ching, J.; Kovalik, J. P.; Kim, J. B., Macrophage VLDLR mediates obesity-induced insulin resistance with adipose tissue inflammation. *Nature communications* **2017,** 8, (1), 1087.
79. Wang, S. W.; Hojabrpour, P.; Zhang, P.; Kolesnick, R. N.; Steinbrecher, U. P.; Gomez-Munoz, A.; Duronio, V., Regulation of ceramide generation during macrophage apoptosis by ASMase and de novo synthesis. *Biochimica et biophysica acta* **2015,** 1851, (11), 1482-9.
80. Skotland, T.; Ekroos, K.; Kavaliauskiene, S.; Bergan, J.; Kauhanen, D.; Lintonen, T.; Sandvig, K., Determining the turnover of glycosphingolipid species by stable-isotope tracer lipidomics. *Journal of molecular biology* **2016,** 428, (24), 4856-4866.
81. Poss, A. M.; Maschek, J. A.; Cox, J. E.; Hauner, B. J.; Hopkins, P. N.; Hunt, S. C.; Holland, W. L.; Summers, S. A.; Playdon, M. C., Machine learning reveals serum sphingolipids as cholesterol-independent biomarkers of coronary artery disease. *The Journal of clinical investigation* **2020,** 130, (3).
82. Poss, A. M.; Holland, W. L.; Summers, S. A., Risky lipids: defining the ceramide score that measures cardiovascular health. *European Heart Journal* **2019**.

Journal Pre-proof

Graphical abstract

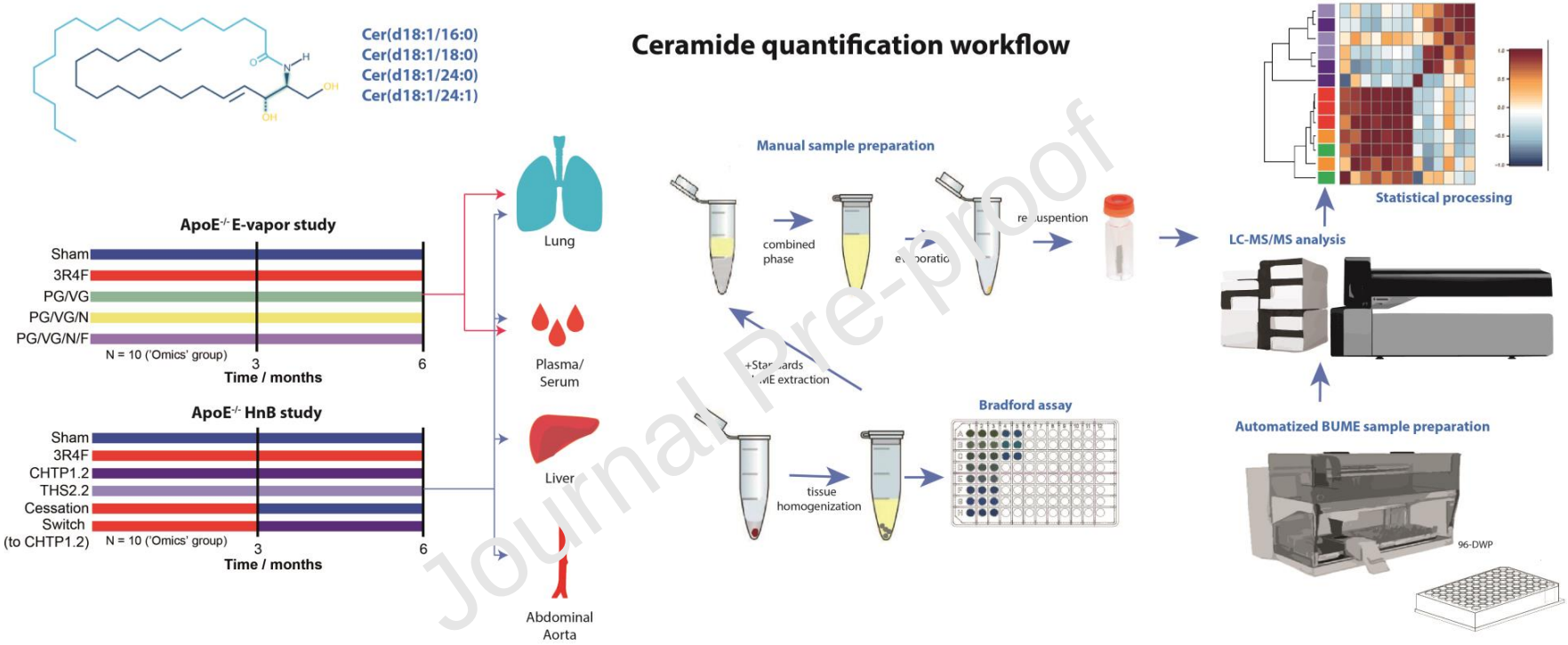

Journal Pre-proof